

Air-Sea fluxes of CO₂ in the Indian Ocean between 1985 and 2018: A synthesis based on Observation-based surface CO₂, hindcast and atmospheric inversion models.

VVSS Sarma¹, B. Sridevi¹, N. Metz², P. K. Patra³, Z. Lachkar⁴, Kunal Chakraborty⁵, C. Goyet^{6,7}, M. Levy², M. Mehari⁴, N. Chandra³

¹CSIR-National Institute of Oceanography, Regional Centre, 176 Lawsons Bay Colony, Visakhapatnam, India

²LOCEAN/IPSL laboratory, Sorbonne Université, CNRS/IRD/MNHN, Paris, France

³Japan Agency for Marine-Earth Science and Technology, Kanagawa, Japan

⁴Arabian Center for Climate and Environmental Sciences, New York University Abu Dhabi, Abu Dhabi, United Arab Emirates

⁵Indian National Centre for Ocean Information Services, Ministry of Earth Sciences, Hyderabad, India

⁶Espace-Dev, UPVD, Perpignan France

⁷Espace-Dev, Univ. Montpellier, UPVD, IRD, Montpellier, France

Abstract

The Indian Ocean significantly influences the global carbon cycle but it is one of the undersampled regions with reference to surface ocean pCO₂. As a part of the Regional Carbon Cycle Assessment and Processes-2 (RECCAP2) project, several approaches, such as interpolated observational climatology, hindcast model, observation-based surface CO₂ (empirical models), and atmospheric inversion models have been employed for estimating net sea-to-air CO₂ fluxes between 1985 and 2018. The seasonal, spatial and long-term variability in sea-to-air fluxes of CO₂ were compared with observational climatology. The mean value of CO₂ in the Indian Ocean (north of 37.5°S) for the period of 1985-2018 using all models is estimated to be -0.19 ± 0.1 PgC yr⁻¹ and it is consistent with the observational climatology (-0.07 ± 0.14 PgC yr⁻¹). The Indian Ocean north of 18°S is found to be the mean annual source (0.04 ± 0.05 PgC yr⁻¹) whereas a net sink (-0.23 ± 0.11 PgC yr⁻¹) in the south of 18°S. All models captured observed spatial patterns but underestimated the net source of CO₂ in the Oman/Somalia upwelling, the Equatorial Indian Ocean (EIO) and the Bay of Bengal (BoB) whereas CO₂ sink is overestimated in the South Indian Ocean (SIO). Overall, all models captured the seasonality in pCO₂ levels and CO₂ fluxes but overestimated the amplitude of their variability. All models suggested the strengthening of the sink over the period between 1985 and 2018 by 0.02 PgC yr⁻¹ decade⁻¹. A significant increase in the collection of surface ocean pCO₂ and atmospheric CO₂ measurements improves the model simulations in the Indian Ocean.

Keywords: Surface pCO₂; CO₂ fluxes; Hindcast models; atmospheric inversions; Indian Ocean

1. Introduction

The atmospheric carbon dioxide (CO₂) levels are ever increasing since the Industrial Revolution due to several anthropogenic activities such as fossil fuel burning and land-use changes. The enhanced anthropogenic activities led to the acceleration of the rate of CO₂ accumulation in the atmosphere from $\sim 1.7 \pm 0.1$ PgC yr⁻¹ in the 1960s to 5.3 ± 0.1 PgC yr⁻¹ in 2021 (Friedlingstein et al., 2022). About half of the total anthropogenic emission remains in the atmosphere, and the remaining half is stored in the ocean and land (Canadell et al. 2021). According to the Global Carbon Project assessment of 2022, the ocean has taken up about 28% (2.9 ± 0.4 PgC yr⁻¹) of the total anthropogenic CO₂ emissions during 2021 (Friedlingstein et al., 2022). It is also well established that the ocean carbon sink increased since the 60s with inter-annual variability (IAV) not fully captured by ocean models.

The Indian Ocean is a small basin compared to the other two major basins of the Pacific and Atlantic and has a unique geography as it is closed in the north at a low latitude. More than 30% of the global population is dwelling along the Indian Ocean coast where rapid industrialization is taking place. As a result, the highest levels of aerosol optical depth (AOD) are observed over the northern Indian Ocean with the highest rate of increase over the globe (Zhang and Reid, 2010; Yadav et al., 2021). The northeastern Indian Ocean (Bay of Bengal; BoB) receives a significant amount of freshwater from major rivers, such as the Ganges, Brahmaputra, and Irrawaddy-Salween systems. The northern Indian Ocean experiences strong seasonality due to a change in direction of monsoonal wind resulting in a reversal in direction of surface currents (Schott and McCreary, 2001), which strongly modulates the biogeochemical cycling of carbon and nitrogen. The northern Indian Ocean is one of the most productive regions in the globe and contributes up to 20% of global ocean primary productivity (Behrenfield and Falkowski, 1997).

Despite the importance of the Indian Ocean in the global carbon cycle, this region is poorly studied with reference to the biogeochemical cycling of carbon compared to the other two major basins. The seasonal cycle of pCO₂ and carbon fluxes was studied only in the Arabian Sea (George et al., 1994; Goyet et al., 1998; Sarma et al., 1998; 2003; 2013, De Verneil et al., 2022; Chakraborty et al., 2021), the BoB (Sarma et al., 2012; 2015; 2020; 2021; Chakraborty et al., 2021) and the south-western Indian ocean (Metzl et al., 1998) whereas the long-term variability was only recently studied in the southwestern Indian Ocean region (Metzl et al., 2022) as the other regions in the Indian Ocean was either sampled once or twice during last few decades (Takahashi et al., 2009; Sarma et al., 2013). The studies carried out in the aegis of the Joint Global Flux Study (JGOFS) and the Bay of Bengal Process Studies (BoBPS) suggested that the seasonal amplitude of pCO₂ goes beyond 200 μ atm in the Arabian Sea (George et al., 1994; Goyet et al., 1998; Sarma et al., 1998; 2003) and BoB (Kumar et al., 1996;

Sarma et al., 2012; 2015; 2019). The large amplitude of variability in $p\text{CO}_2$ is driven by variabilities in physical transport, such as upwelling, and convective mixing, in the Arabian Sea, whereas freshwater input by rivers and atmospheric pollutants deposition in the BoB (Sarma et al., 2000; 2012). River discharge displays significant inter-annual variability (Papa et al., 2012). Sarma et al. (2012) found that peninsular rivers bring acidic and high $p\text{CO}_2$ waters to the coast whereas glacial rivers, such as Ganges and Brahmaputra, bring relatively basic and low $p\text{CO}_2$ waters to the BoB. Therefore, the source of river water determines the direction of the flux of CO_2 at the air-sea interface. Kumar et al. (1996) suggested that the BoB is a sink for atmospheric CO_2 in the 1990s whereas Sarma et al. (2015; 2021) found that it is a mild source of the atmosphere due to the deposition of atmospheric pollutants. More recently Sridevi and Sarma (2021) indicated that salinity in the surface waters of the BoB is decreasing over the past two decades due to an increase in the warming of Himalayan glaciers (Goes et al., 2020). Since the pH of the Ganges and Brahmaputra River waters are relatively basic (Sarma et al., 2012), an increase in pH and a decrease in $p\text{CO}_2$ was noticed in the past two decades in the central and eastern BoB (Sridevi and Sarma, 2021).

Unlike the other two major basins, upwelling is weak in the equatorial Indian Ocean due to the prevalence of westerly winds along the equatorial Indian Ocean (Schott et al., 2009). A flat thermocline is observed in the equatorial Indian Ocean in the east-west direction (Murtugudde and Bualacchi, 1999; Xie et al., 2002). The southern tropical and subtropical region is influenced by the inflow of Pacific waters from the Indonesian Through Flow (ITF) (Schott and McCreary, 2001). A major subduction zone occurs in the South Indian Ocean between 15 and 50°S due to positive wind stress curl (Schott et al., 2009). The subducted water masses are advected to the northern Indian Ocean (Miyama et al., 2003; Schott et al., 2002), carrying nutrients and anthropogenic CO_2 (Sabine et al., 1999). A perennial sink of atmospheric CO_2 was reported in the south Indian Ocean (SIO; Metzl et al., 1991; Poisson et al., 1993; Metzl et al., 1995; 1998; 2022; Metzl, 2009).

The Indian Ocean experiences strong zonal variability driven by the Indian Ocean Dipole/Zonal Mode (IOD/IODZM) in addition to El Nino-Southern Oscillation (ENSO) and the Southern Annular Mode (SAM) (Saji et al., 1999; Murthugude et al., 2000; Thompson and Solomon, 2002). These climate modes of variability modulate several physical and biogeochemical processes resulting in significant modifications in the CO_2 flux (Sarma 2006; Valsala et al., 2020). The influence of SAM was suggested in the SIO for the period 1991-2007 with large spatial variability in CO_2 growth rate with lower rates in the north of 40°S than south of 40°S during austral winter but higher and uniform rates during austral summer (Metzl, 2009).

Gruber et al. (2009) identified a significant mismatch between top-down and bottom-up inversion in the tropical Indian Ocean and attributed it to a lack of atmospheric CO₂ data. Sarma et al. (2013) compared CO₂ fluxes from the Indian Ocean between 1990 and 2009 using a suite of models (both ocean biogeochemistry and atmospheric inversions) under the aegis of the RECCAP1 project. For the band 30°N-44°S, the median annual sea-air CO₂ flux from models was -0.37 ± 0.06 PgC yr⁻¹ and it was consistent with -0.24 ± 0.12 PgC yr⁻¹ using observations. They further noticed that although all models captured the spatial patterns, CO₂ outgassing was underestimated in the upwelling region and overestimated sink in the BoB, whereas CO₂ uptake was underestimated in the subtropical convergence zone.

Recent use of regional models to study the dynamics of regional ecosystems and biogeochemical cycles in the Indian Ocean revealed an improved representation of key processes relative to global coarse resolution models. For instance, the representation of oxygen minimum zones (OMZ) in the northern Indian Ocean indicates large discrepancies with observations in both CMIP5 and CMIP6 global models, but shows a much-improved agreement with data in regional model simulations, both in terms of their structure, size and intensity (Bopp et al., 2013, Cocco et al., 2013, Kwiatkowski et al., 2020, Al Azhar et al., 2017, Lachkar et al., 2016, 2018, 2021). This was linked to the importance of eddy fluxes - typically inaccurately parameterized in global coarse-resolution models but resolved in finer-resolution regional models – in shaping OMZs (e.g., Lachkar et al., 2016, Bettencourt et al., 2015, Brandt et al., 2015, Chakraborty et al., 2019). Furthermore, accurately representing the structure and intensity of these low-O₂ bodies in regional models is critical to represent their recent and future changes under ongoing climate change (Lachkar et al., 2021). Mesoscale eddies were also shown to have a significant impact on the carbon cycle in the northern Indian Ocean (Sarma et al., 2016; 2019; 2021). Additionally, significant improvements in parameterizations of river discharge, monsoon mixing and associated biological response in the high-resolution regional models lead to a better representation of the upper ocean cycle in the regional models (Chakraborty et al., 2018; 2021; Ghosh et al., 2022; Valsala et al., 2021). Therefore, eddy-resolving regional models may lead to an improved representation of the carbon cycle in the region. This work aims to evaluate the net air-sea CO₂ fluxes by different global and regional models and quantify how these simulated net CO₂ fluxes in the Indian Ocean are comparable with observational climatology and identify potential reasons for deviations, if any, in the Indian Ocean.

2. Methods

2.1. Study region

Based on the RECCAP2 regional definitions, the entire Indian Ocean, north of 37.5°S, was considered as one region. Due to the complexity of the regional physical processes in the Indian Ocean, we define here the following five regions for analysis: i) the entire Indian Ocean (30°N-37.5°S), ii) the Arabian Sea (0-30°N; 38-78°E), iii) the Bay of Bengal (BoB; 0-30°N; 78-110°E), iv) Equatorial Indian Ocean (EIO; 0-18°S) and v) South Indian Ocean (SIO; 18°S-37.5°S) (Figure 1a).

2.2 Data sets

To describe the regional CO₂ fluxes for the Indian Ocean, RECCAP2 global CO₂ flux products were used that include observations (climatology referenced to the year 2000; Takahashi et al., 2009), Global hindcast (GHM), regional hindcast (RHM) models, observation-based (empirical) surface pCO₂ models and atmospheric inversion models.

2.2.1. Observational climatology

The Indian Ocean is one of the least sampled basins in the world ocean for surface pCO₂ measurements with reference to space and time (Figure 1b; Bakker et al., 2016). The major addition of data was done during 1990-1999 whereas in the next decade (2000-2009) some data were added in the SIO and one transect in the BoB and good coverage of the Bay was done in 2010-2019 (Bakker et al., 2020; Supplementary Figure S1). Within the Indian Ocean, the seasonal and inter-annual pCO₂ data are available in the western basin (the Arabian Sea and the southwestern Indian Ocean). In contrast, only 2 to 3 times were sampled in the eastern basin (Supplementary Figure S1). In addition to this, time-series pCO₂ (water and air) data are available in the central BoB, as a part of the RAMA (Moored array for African-Asian-Australian Monsoon Analysis and Prediction) buoy program (BOBOA, Sutton et al., 2019), from 2013 onwards (Figure 1). Nevertheless, understanding seasonality in pCO₂ is a challenge in the Indian Ocean due to the weak spatial and seasonal data coverage. Takahashi et al. (2009) (Figure 1c) compiled the available pCO₂ data in the Indian Ocean and gridded it to 4° x 5° using two-dimensional advection-diffusion equations to interpolate with reference to space and time. The major challenge here is that the observations (henceforth called climatology) are not absolutely observations alone but were interpolated in the regions where data were unavailable. There is uncertainty associated with the techniques used for developing climatology. Due to the lack of seasonal data in some regions, the seasonality shown in the data is significantly driven by the model used to interpolate. However, the performance of the seasonality driven by the model used to derive climatology is tested using pCO₂ data generated by the BOBOA buoy in the central BoB. Nevertheless, the observed CO₂ fluxes carry several errors due to sparse coverage of data, wind speed measurements

and transfer velocity parameterizations and the uncertainty of the CO₂ fluxes is about 50% (Gruber et al., 2009).

Since RECCAP1 (Sarma et al., 2013) important progress has been made on both pCO₂ data delivery each year in the public domain for updating SOCAT data-product (www.socat.info, Pfeil et al., 2013; Bakker et al., 2014, 2016) and the development of empirical methods that reconstruct pCO₂ fields, including in synthesis studies (SOCOM project, Rödenbeck et al., 2015). Here we used 9 empirical methods based on the SOCAT data (version v2020) and to compare our new results with RECCAP1, we also used the original climatology of Takahashi et al (2009) (Figure 1c). Recall that climatology was constructed for the reference year 2000 which would have to be taken into account when comparing pCO₂ fields for the recent year. However, this would not dramatically impact the mean CO₂ fluxes assuming that over 1985-2018 ocean pCO₂ increase is close to the atmospheric growth rate as observed in some parts of the Indian Ocean (e.g. Metzl, 2009; Lauvset et al., 2015; Metzl et al., 2022; Lo Monaco et al., 2021).

2.2.2. Ocean Hindcast models

CO₂ fluxes and surface water pCO₂ data were obtained from 12 GHM and 2 RHM (Table 1). These models represent physical, chemical and biological processes controlling the marine carbon cycling and exchange of CO₂ at the sea-to-atmosphere interface. The GHM have a coarse or an eddy-permitting horizontal resolution whereas RHM is eddy-resolving (Table 1). The simulations are forced with meteorological reanalysis products, given in Table 1. The models were run for different periods mostly between 1980 and 2019 with the period of each model given in Table 1. In order to make it uniform for all models, we have considered the runs between 1985 and 2018 in this study that gives the reference year of 2002. GHM and RHM have been integrated from the pre-industrial period to the present day with the same atmospheric CO₂ history. Although the model simulations were carried out following the RECCAP2 ocean modelling protocol, each model is different from others with respect to forcing, experimental configuration, representation of biogeochemical processes and sub-grid parameterizations (Table 1).

2.2.4. Atmospheric inversions

Atmospheric inversions (top-down) estimate the surface CO₂ fluxes based on the variability in the measured atmospheric CO₂ using an atmospheric transport model. In the atmospheric inversion models, a priori information about the surface CO₂ fluxes is used from bottom-up estimates (e.g., Takahashi et al., 2009) or an ocean GHM or an empirical upscaling model. In the Indian Ocean region and surrounding, atmospheric CO₂ measurements are available from only 8 sites that are used in the

atmospheric inversion models. Among them, only two stations have long-record and others have short records. However, most inversions did not correct the oceanic prior fluxes significantly when the empirical upscaling model fluxes were used. Here we have chosen to show sea-air CO₂ fluxes from inversion models, one using prior flux from Takahashi et al. (2009) in the MIROC4-ACTM system (Chandra et al., 2022) and the other model (CAMsv20r1) using prior fluxes from an empirical model (Chevallier et al., 2005). The atmospheric inversion model runs are available between 2001 and 2018 which gives the reference year of 2009.

2.2.5. Observation-based Surface pCO₂ (Empirical models)

Global sea-air CO₂ fluxes can also be estimated from pCO₂ measurements along the ship tracks over the past several decades. The first and simple upscaling method was implemented by Takahashi et al. (2009) where all the past measurements of CO₂ are separated in monthly-mean flux maps based on SST and salinity. This method relied on the extrapolation of Delta_pCO₂ data from limited measurements along the cruise tracks to the global ocean. With the development of neural networks and other artificial intelligence tools and organised archival of the SOCAT CO₂ database, several methods are now implemented to calculate gridded CO₂ flux including the interannual variation, taking into account the physical state of sea-surface conditions (Table 2; Rödenbeck et al., 2015; Landschützer et al., 2016; Fay et al., 2021). The estimated CO₂ fluxes between 1985 and 2018 were considered in this study with the reference year of 2002.

3. Results and Discussion

The simulations of CO₂ uptake by the Indian Ocean by GHM, RHM, empirical and atmospheric inversion models are compared with climatology with reference to (i) annual, (ii) seasonal and (iii) interannual timescales.

3.1. Annual mean CO₂ fluxes in the Indian Ocean between 1985 and 2018

3.1.1. Tropical Indian Ocean (north of the 37.5°S)

The annual mean sea-air CO₂ fluxes for 1985 to 2018 are presented in Table 3 and Figure 1d for the entire Indian Ocean (37.5°S –30°N; 25-125°E), Arabian Sea (30-78°E and 0-30°N), BoB (78-110°E and 0-30°N), EIO (30-125°E, 0-17°S) and SIO (37.5-17°S and 25-130°E). The spatial variability in mean annual uptake for the entire Indian Ocean by GHM and RHM (Figure 2), empirical (Figure 3) and atmospheric models (Figure 4) are given to evaluate the spatial variability in CO₂ fluxes.

The simulated mean annual CO₂ sea–air fluxes by different models varied between -0.27 and -0.13 PgC yr⁻¹ for the Indian Ocean (Table 3), with a relatively lower sink estimated by empirical models (-

0.13 ± 0.04 PgC yr⁻¹) than hindcast (-0.21 ± 0.10 PgC yr⁻¹) and atmospheric inversion models (-0.27 ± 0.16 PgC yr⁻¹). Both hindcast and atmospheric inversion models overestimated the sink of CO₂ by 3 times that of climatology (-0.07 ± 0.14 PgC yr⁻¹) whereas empirical models are close to the observations. The observational pattern of CO₂ flux shows that the SIO is a dominant sink whereas the Arabian Sea is a strong source while EIO and the BoB are weak sources of atmospheric CO₂. All models simulated similar patterns of spatial variations of the CO₂ fluxes (Figures 2 to 4) that are in agreement with observations, but the magnitudes of fluxes are different. For instance, the modelled CO₂ fluxes were spread around the climatological values with relative overestimation of the sink in the south of 22°S, in contrast, underestimation of the source was noticed by all models in the north of 22°S in the Indian Ocean. In contrast, the RHM (both INCOIS-BIO-ROMS and ROMS_NYUAD) reproduced CO₂ fluxes well in comparison with the climatology. Since the ROMS_NYUAD model simulation was submitted up to 31.5°S only, we did not include it in the SIO region as it was considered up to 37.5°S for other models. Similarly, the simulated CO₂ fluxes by empirical models are in good agreement with the climatology (Figure 3). In the case of the atmospheric inversions, a higher CO₂ sink in the south of 15°S whereas sources of CO₂ in the north of 15°S than the observational climatology was observed (Figure 4). The CO₂ fluxes by all models are in near perfect agreement with each other for the entire Indian Ocean within the standard deviation of the estimates, however, they are different on the regional subdivisions such as the Arabian Sea, BoB, EIO and SIO.

The standard deviation for the atmospheric inversion was large in the annual uptake (-0.27 ± 0.16 PgC yr⁻¹) while the smallest for the empirical models (-0.13 ± 0.04 PgC yr⁻¹; Table 3). The highest standard deviation in the atmospheric inversion comes from the sparse atmospheric CO₂ measurements, transport model uncertainties and differences in the prior flux assumptions for the Indian Ocean. The atmospheric CO₂ time series data are available only at 8 locations within the Indian Ocean resulting in high variability in the estimates. The climatology also has a very high standard deviation (-0.07 ± 0.14 PgC yr⁻¹) due to a lack of enough data in the Indian Ocean as most of the Indian Ocean region is either sampled once or twice and inter and extrapolation of the data (Takahashi et al., 2009).

The zonal integrated CO₂ fluxes by different models are given in Figure 5 and it shows that most of the GHM underestimated CO₂ sink in the south of 25°S whereas over estimated north of 25°S. The RHM (INCOIS-BIO-ROMS and ROMS_NYUAD) simulated exceptionally well the zonal mean CO₂ fluxes in the Indian Ocean between 37.5°S and 27.5°N. However, a slight underestimation was noticed for both the RHM and GHM in the north of 5°N (Figure 5a). In the case of empirical models (Figure 5b), Jena-MLS, JMAMLR and UOEX_WAT20 were over-estimated in the south of 15°S and well performed in the north of 15°S with reference to climatology. In the case of atmospheric inversions, a

stronger sink is noticed in the south of 15°S and a stronger source in the north of 10°S, compared to the empirical and hindcast models (Figure 5c).

Both spatial variations and zonal integration in the CO₂ fluxes (Figures 2-5) suggest that the model simulations significantly deviated from the climatology at several zones, namely the Oman/Somali upwelling region in the Arabian Sea, freshwater discharge region in the BoB, equatorial upwelling region and south equatorial current (SEC) and subtropical convergence zone regions in the southern tropical Indian Ocean. The potential reasons responsible for the regional variations in the CO₂ fluxes were discussed in detail below.

3.1.2. Northwestern Indian Ocean (Arabian Sea)

The Arabian Sea is simulated as a net source of CO₂ to the atmosphere by the hindcast models (0.006 to 0.058 PgC yr⁻¹ with a mean of 0.03±0.01 PgC yr⁻¹), empirical models (0.052 to 0.098 with a mean of 0.08±0.01 PgC yr⁻¹) and atmospheric inversions (0.16±0.12 PgC yr⁻¹; Table 3) and it is consistent with the observations (Sarma, 2003; Goyet et al., 1998; Millero et al., 1998) and climatological fluxes (0.08±0.06 PgC yr⁻¹) (Table 3). Considering the standard deviation of climatology, and models, the mean of all modelled fluxes in the Arabian Sea (0.06±0.05 PgC yr⁻¹) is close to that of climatology (0.08±0.06 PgC yr⁻¹; Table 3). The large source of CO₂ to the atmosphere from the Indian Ocean is driven by the upwelling off Oman/Somali coasts, where pCO₂ levels as high as >600 µatm were reported during the peak southwest monsoon period (Körtzinger et al., 1997; Goyet et al., 1998; Sarma, 2003; Sabine et al., 2000). Most of the models poorly simulated CO₂ fluxes in the Oman/Somali upwelling region (Figures 2-4). Within the hindcast models, both MRI-ESM2-1 and ROMS_NYUAD models simulated CO₂ fluxes close to the observations (Figure 2).

The simulation of upwelling in the Arabian Sea may be a challenge due to the complex interplay of winds, bottom topography, monsoonal circulation and mixing, to capture the observed response by the models. The monsoon mixing is intense during summer (June to September) resulting in high pCO₂ levels in the entire Arabian Sea with maximum off Oman and Somalia coasts (Sarma et al., 1996; 1998; Goyet et al., 1998; Körtzinger et al., 1997). It was estimated that the mixing effect is a dominant controlling factor of surface ocean pCO₂ in the Arabian Sea during the monsoon period while biological effect, mainly bacterial degradation, dominates during the non-monsoon period (Louanchi et al., 1996; Sarma et al., 2000). All hindcast models failed to simulate the monsoon mixing well resulting in weaker fluxes of CO₂ (Figure 2) to the atmosphere. Since empirical models are mainly driven by observations, they could simulate the impact of upwelling on pCO₂ reasonably well (Fig. 3). In the case of atmospheric models, MACTM over-estimated coastal upwelling whereas CAMSv20r1

remained close to that of the prior flux field from CEMES_LSCE_FFNN (Figure 4). Sarma et al. (2013) noticed weak mixing in the GHM, and ocean inversion models in the Arabian Sea between 1990 and 2009 and no improvements were noticed with reference to mixing in the Arabian Sea in the past decade.

To examine the variability in the simulation of mixing in the Oman/Somalia upwelling regions by different GHM and RHM, the sea surface temperature (SST) simulated by the hindcast models was compared (Supplementary Figure S2). All models simulated upwelling features off Oman/Somalia region, however, the intensity of mixing was different among models, as reflected in the SST. It was noticed that mixing was weaker in CCSM-WHOI, EC-Earth3, MOM6-Princeton, NorESM-OC1.2, ORCA025-GEOMAR and Planktom12 models than in other GHM as former models showed relatively warmer SSTs than later models compared to the climatology. Since a significant amount of data was contributed to the climatology from the Oman/Somali upwelling region, we can confidently attribute that the mixing and pCO₂ input from the subsurface layers in the Oman/Somalia upwelling region needs to be improved in the GHM for accurate simulations.

3.1.3. Northeastern Indian Ocean (Bay of Bengal)

All models simulated that the BoB is a mild source of CO₂ (0.00 to 0.01 PgC yr⁻¹ with a mean of 0.00±0.01 PgC yr⁻¹) and it is consistent with the climatology (0.01±0.01 PgC yr⁻¹; Takahashi et al., 2009; Table 3). Sarma et al. (2012) reported that the peninsular river discharge increased the pCO₂ levels whereas glacial rivers (Ganges and Brahmaputra) discharge decrease the pCO₂ levels (Kumar et al., 1996; Mukhopadhyay et al., 2002). More recently Sarma et al. (2019) reported that cyclonic eddies enhance pCO₂ levels due to upwelling in the core of the eddy while anticyclonic eddies sink for atmospheric CO₂. Several recent investigations suggested that rapid acidification is being occurred in the BoB due to the deposition of atmospheric pollutants (Sarma et al., 2015; 2021; Kumari et al., 2022a,b) leading to an increase in pCO₂ levels. Unfortunately, neither GHM nor RHM has the atmospheric component to consider its impact.

Since river discharge enhances the CO₂ sink to the BoB, the differences in the sink of CO₂ in the BoB may be caused by variable use of river discharge data as this would influence the salinity of the upper ocean in the BoB. The existence of a strong linear relationship between salinity and pCO₂ levels was reported in the BoB (Kumar et al., 1996; Sarma et al., 2012; 2021). Recently, Sridevi and Sarma (2021) observed decreasing trends in surface pCO₂ levels due to a decrease in salinity over the past two decades due to the warming of Himalayan glaciers (Goes et al., 2020). Therefore, salinity is a crucial parameter in controlling the pCO₂ levels in the BoB.

To examine this, the salinity simulations by different models were examined (Supplementary Figure S3). All GHM simulated low salinity in the northern Bay but the magnitude of salinity is different in the north of 15°N. The lower salinity in the northern Bay was simulated in CCSM-WHOI, MOM6-Princeton and ORCA1-LIM3-PISCES, whereas relatively high salinity was simulated in CNRM-ESM2-1 and Planktom12. However, the sink in CO₂ was observed in both high and low-salinity simulated models suggesting that variability in the sink of CO₂ is not caused by river discharge/salinity in the GHM. An insignificant relationship was observed between salinity and pCO₂ levels among different GHM and RHM in the northern BoB (Figure is not shown) suggesting salinity or river discharge may not be a controlling factor on variable CO₂ fluxes in the BoB. The absence of a relationship between salinity and pCO₂ levels in the models suggests that the role of freshening surface waters by rivers was not well constrained in the hindcast models.

3.1.4. Equatorial Indian Ocean (EIO)

The empirical models (0.02 ± 0.02 PgC yr⁻¹) and atmospheric inversions models (0.02 ± 0.03 PgC yr⁻¹) simulated a mild source of the atmospheric CO₂ and it is consistent with the climatology (0.04 ± 0.03 PgC yr⁻¹), in contrast, hindcast models estimated sink (-0.05 ± 0.04 PgC yr⁻¹) in the EIO. All models simulated that the western equatorial Indian Ocean is a source whereas the eastern region is either a sink or close to balance. The higher sink simulated by GHM is caused by weaker Somalia upwelling as discussed in section 3.1.2. RHM simulated that the equatorial Indian Ocean is a mild source of atmospheric CO₂ (0.01 ± 0.06 and 0.03 ± 0.08 PgC yr⁻¹ by ROMS-NYUAD and INCOIS-BIO-ROMS respectively). This can be noticed from the spatial distribution of SST, which is relatively warmer in the GHM in the western equatorial region compared to the RHM (Supplementary Figure S4) suggesting better simulation of upwelling in the RHMs. The spatial variations in CO₂ fluxes by RHM and atmospheric inversions (Figures 2 and 4) are consistent with the observations in the EIO region (Figure 1c).

3.1.5. The South Indian Ocean (SIO)

The SIO comprises two key oceanographic regimes of oligotrophic waters in the north and Southern Ocean waters in the south. These two regions are separated by the subtropical front (STF). We have considered the STF region as part of the SIO in this study. The estimated mean fluxes in this region by all models are -0.23 ± 0.11 PgC yr⁻¹ suggesting a strong sink of atmospheric CO₂ that agrees well with climatology (-0.20 ± 0.16 PgC yr⁻¹; Table 3). The atmospheric inversions estimated a larger sink (-0.46 ± 0.3 PgC yr⁻¹), which is mainly caused by MATCM whereas the CAMSv20r1 model performed well by staying close to the prior model. Despite atmospheric observations available in the SIO at

Amsterdam Island at 38°S, the overestimation of the sink by the atmospheric model must be examined. Both empirical models (-0.22 ± 0.04 PgC yr⁻¹) and hindcast models, including RHM, (-0.20 ± 0.07 PgC yr⁻¹) estimated CO₂ fluxes close to that of climatology (-0.22 ± 0.04 PgC yr⁻¹). The CO₂ fluxes in the SIO are closer in magnitude to the annual uptake for the entire Indian Ocean (-0.19 ± 0.1 PgC yr⁻¹) indicating that the majority of the net uptake of CO₂ occurs in the SIO, as suggested by other studies (Sabine et al., 2000; Bates et al., 2006; Metzl, 2009; Takahashi et al., 2009; Sarma et al., 2013).

The spatial variability in the magnitude of CO₂ flux within the SIO was variable among hindcast models (Figure 2) in comparison to climatology (Figure 1c). For instance, the climatology suggests a strong sink between 15°S and 35°S whereas the sink was simulated by most of the hindcast models between 10°S and 25°S. Sabine et al. (1999) observed the highest concentration and deepest penetration of anthropogenic carbon in the subtropical convergence zone (30-40°S). In contrast, a mild source is simulated by most of the models in the south of 30°S suggesting that the sink was underestimated in this zone. The outcropping of these density surfaces and the subsequent sinking of surface waters provide a pathway for excess CO₂ to enter the interior of the ocean. Overestimation of the CO₂ uptake by the models in these zones suggests that vertical mixing was not constrained properly in the models, leading to excess deep mixing, which increased surface water pCO₂ and a decrease in the flux of the ocean (Figure 2).

3.2. Seasonal variations in pCO₂ levels and air-sea CO₂ fluxes in the Indian Ocean

To examine the seasonal variability of CO₂ fluxes by various modelling approaches, the simulated surface pCO₂ levels and CO₂ fluxes were analysed (Figure 6). This provides insights into the ability of the models to represent the complex interplay of physical and biological processes on pCO₂ levels and sea-air CO₂ exchange. The ability of a model to reproduce the seasonal cycle also provides some reassurance that the models are correctly projecting climate sensitivity of the processes that could influence long-term projections of the ocean CO₂ uptake (Fig. 6).

3.2.1. The Entire Indian Ocean

The increase in pCO₂ levels is expected in the tropical Indian Ocean between June and September due to an increase in mixing driven by the southwest monsoon in the north whereas deeper mixing in the SIO (Louanchi et al., 1996; Sarma et al., 2000; Sabine et al., 2000; Bates et al., 2006). All hindcast models overestimated the sink between June and September but were close to observation during other months (Fig. 6) due to weak mixing of pCO₂-rich subsurface waters with surface. Among the other models, ROMS-NYUAD and MPIOM-HAMOCC displayed relatively better seasonality in CO₂ fluxes compared to climatology (Figure S5). The mean empirical models followed seasonality close

to that of observations. The atmospheric inversions overestimated the sink from March to October mainly in the SIO compared to other models and climatology. Since the seasonality in CO₂ fluxes is variable with space, the same in different regions of the Indian Ocean are examined.

3.2.2. Northwestern Indian Ocean (Arabian Sea)

The Arabian Sea shows strong seasonality with higher CO₂ fluxes from June to September associated with monsoon mixing and high winds compared to other seasons (George et al., 1994; Sarma et al., 1996; 1998; Sarma, 2003). The climatological amplitude of seasonality was close to 0.2 PgC yr⁻¹ with a maximum in June-August and a minimum in October-December (Figure 6). The seasonality was perfectly captured by the empirical models whereas atmospheric inversion and hindcast models failed to simulate as they over and underestimated respectively. Though atmospheric inversion models mostly captured the high CO₂ fluxes to the atmosphere from June to August but with a large spread compared to other simulations by hindcast and empirical models. In contrast, hindcast models showed a response but it was strongly out of phase with the observations by giving maximum fluxes in May to June and minimum fluxes in July to September with approximately 3-4 months ahead of the climatological peak in CO₂ fluxes. The two GHM (MRI-ESM2-1 and NorESM-OC1.2) and RHM (ROMS-NYUAD) simulated peak fluxes between June and August in the Arabian Sea (Figure S5).

All GHM failed to simulate seasonality in pCO₂ (Figure 6) levels as the higher pCO₂ levels were observed during July to September in the observations whereas April to May in the models. High pCO₂ levels were reported from June to August due to enhanced vertical mixing caused by monsoon winds in the Arabian Sea (Sarma et al., 1996; 1998; Körtzinger et al., 1997; Millero et al., 1998; Sarma, 2003). Sarma et al. (2000) observed that mixing is the dominant controlling factor of pCO₂ levels from June to August in the Arabian Sea followed by biological effects (Louanchi et al., 1996; Goyet et al., 1998). The difference in pCO₂ levels between mean hindcast models and observations varied between 15 and 50 µatm whereas it was <20 µatm in the case of empirical models (Figure 6). The reference year for climatology is 2000 (Takahashi et al., 2009) whereas the reference year for hindcast and empirical models are 2002 (1985-2018). The difference in pCO₂ levels caused by variable reference year may differ up to 4 µatm considering the 2 µatm/y as a growth rate of surface ocean pCO₂ (Metzl, 2009) suggesting that weaker mixing in the models underestimated the seasonality in pCO₂ and CO₂ fluxes in the Indian Ocean.

3.2.3. Northeastern Indian Ocean (Bay of Bengal; BoB)

The BoB also displayed large seasonality with higher CO₂ fluxes from May to August associated with monsoon mixing and decreased between October and December due to river discharge and

stratification (Figure 6; Sarma et al., 2016; 2018; 2019). All models simulated high CO₂ fluxes during May but decreased to low by July-August (Figure 6). The observed amplitude of seasonality was close to 0.02 PgC yr⁻¹ with the maximum in May-June (0.02 PgC yr⁻¹) and minimum in February (0 PgC yr⁻¹). The mean hindcast models simulated similar amplitude (0.02 PgC yr⁻¹) but they showed sink (0 and -0.02 PgC yr⁻¹) instead of source in the climatology. The atmospheric inversion models displayed too low (high sink during February) and high source from August to October.

All GHM simulate seasonality in pCO₂ levels in the BoB with a maximum in April and May and a minimum in February (Figure 6). The magnitude of seasonal variability in pCO₂ is ~15 µatm in the climatology whereas hindcast models simulated 15-40 µatm with lower variability (<20 µatm) during April and May and higher (>35 µatm) during other months. The underestimation of pCO₂ in the BoB may be caused by strong stratification in the model leading to lower input from pCO₂-rich subsurface waters. In addition to this, the difference between simulations and observation may also be caused by the lack of enough data in the observations as the BoB is severely under-sampled with reference to seasons. To resolve this issue, the pCO₂ data collected by the BOBOA mooring buoy in the central BoB (Figure 1a) is used for comparison. This buoy collected data between 2013 and 2018 (Sutton et al 2019) and the monthly climatology of this data was compared with Takahashi climatology. The BOBOA climatology showed an increase in pCO₂ starting in April with a peak in May whereas Takahashi climatology displayed during April suggesting that Takahashi climatology well reproduced the observed seasonality although the climatology was not constrained with BOBOA data. Most of the hindcast models displayed peaks in April-May in the BoB and were also consistent with the climatology (Figure S5).

3.2.4. Equatorial Indian Ocean (EIO)

The CO₂ fluxes in the EIO displayed seasonality with high fluxes from January to May and low from June to October with a minimum in August (Figure 6). The mean observed CO₂ fluxes are the source of the atmosphere during all seasons whereas all hindcast models simulated sink, especially between May and November. All models displayed similar seasonal variability in CO₂ fluxes but underestimated from May to November. The RHM simulated better seasonality in the CO₂ fluxes compared to GHM (Figure S5).

The EIO displays relatively weak pCO₂ seasonality with a high from February to April and a low from June to October. The amplitude of seasonality in pCO₂ was <10 µatm in the climatology. All models simulated the seasonality but they were under-estimated pCO₂ by ~20 µatm from that of climatology (Figure 6).

3.2.5. The South Indian Ocean (SIO)

The SIO displayed large seasonality in fluxes with CO₂ source during January to March and CO₂ sinks during other months (Figure 6). All models reproduced seasonality very well in the SIO (Figure S5).

All GHM simulate seasonality in pCO₂ levels in the SIO with a maximum in January and March and a minimum in July-August. The magnitude of seasonal variability in pCO₂ is ~15 µatm in the climatology whereas hindcast models simulated <20 µatm. The difference in pCO₂ between simulation and observations was up to 40 µatm (Figure S5). The large difference in pCO₂ seasonality in the SIO may be caused by weaker mixing simulations in the models in austral winter and the opposite in summer.

3.3. Interannual variability (IAV)

The interannual variability and trends in pCO₂ levels and their fluxes at the air-water interface was also investigated in 1985-2018 using different models (Figure 7). The rate of increase in surface ocean pCO₂ levels varied from 1.54 to 1.73 µatm yr⁻¹ between 1985 and 2018 with a lower rate of increase in the BoB and higher in the EIO and SIO. The growth rate of pCO₂ in the surface waters by both hindcast and empirical models is close to that of atmospheric growth and observed surface pCO₂ growth in the Southwestern Indian Ocean (Metzl, 2009; Lo Monaco et al., 2021; Leseurre et al., 2022). Due to the lack of basin-scale observational time-series data in the Indian Ocean, the performance of the IAV by the models cannot be assessed. Given the variability of IOD and ENSO index (Figure 7), we divided the IAV trends into three timelines, i.e., a) 1985-2000, b) 2001-2018 and c) 1985 to 2018 (Figure 7; Tables 4 and 5) to examine the possible changes in growth rate in the recent decades from that of earlier. To avoid biasing the magnitude of the seasonality, we first de-trend the simulated time series of IAV.

3.3.1. The entire Indian Ocean

Both hindcast and empirical models simulated IAV in the surface pCO₂ levels in the entire Indian Ocean as 1.67 to 1.70 µatm yr⁻¹ between 1985 and 2018. The rate of increase in pCO₂ levels was lower from 1985 to 2000 (1.41-1.49 µatm yr⁻¹) and increased in the recent decades (2001-2018) to 1.84-1.96 µatm yr⁻¹ (Table 4). Within the variability in the estimations, both empirical and hindcast models simulated similar growth rates in pCO₂ levels (Figure 7).

The range of sea-to-air CO₂ fluxes for the period of 1985 to 2018 was significantly different for GHM (-0.48 to -0.06 PgC yr⁻¹), empirical (-0.31 to 0.03 PgC yr⁻¹) and atmospheric inversion models (-0.63

to 0.09 PgC yr^{-1}) (Figure 7). The IAV trend between 1985 and 2018 was close for hindcast ($-0.023 \pm 0.003 \text{ PgC yr}^{-1} \text{ decade}^{-1}$) and empirical models ($-0.021 \pm 0.003 \text{ PgC yr}^{-1} \text{ decade}^{-1}$; Table 5). The trends in IAV by hindcast models between 2001 and 2018 ($-0.023 \pm 0.007 \text{ PgC yr}^{-1} \text{ decade}^{-1}$) were slightly lower compared to 1985-2000 ($-0.028 \pm 0.012 \text{ PgC yr}^{-1} \text{ decade}^{-1}$) for the entire Indian Ocean suggesting the rate of sinking of CO_2 in the Indian Ocean is decreasing in the recent decades. In contrast, empirical models displayed larger IAV between 2001-2018 ($-0.046 \pm 0.005 \text{ PgC yr}^{-1} \text{ decade}^{-1}$) and 1985-2000 ($+0.007 \pm 0.007 \text{ PgC yr}^{-1} \text{ decade}^{-1}$). Such differences in the empirical models may come from the lack of satellite Chl-a data before 1998. Therefore, the simulations of empirical models may be less accurate before 1998 than after. Interestingly IAV by empirical models during 2001-2018 were more than double ($-0.046 \pm 0.005 \text{ PgC yr}^{-1} \text{ decade}^{-1}$) than that of hindcast models ($-0.023 \pm 0.007 \text{ PgC yr}^{-1} \text{ decade}^{-1}$) which may be driven by variability in wind products and transfer velocity coefficients used. To examine the spatial variability in IAV, the same is studied in different regions of the Indian Ocean.

3.3.2. Northwestern Indian Ocean (Arabian Sea)

The pCO_2 growth of 1.64 to $1.68 \mu\text{atm yr}^{-1}$ was simulated between 1985 and 2018 and it was lower during 1985-2000 (1.32 - $1.41 \mu\text{atm yr}^{-1}$) than 2001-2018 (1.76 - $1.88 \mu\text{atm yr}^{-1}$) (Table 4) in the Arabian Sea. The growth rates in pCO_2 levels in the Arabian Sea are close to that of the atmospheric growth rate of CO_2 (WMO Bulletin; <https://gml.noaa.gov/ccgg/trends/>).

The IAV in the CO_2 fluxes by the hindcast models in the Arabian Sea was small (0.00 to 0.06 PgC yr^{-1}), it was larger than the mean flux to the atmosphere from 1985 to 2018 ($0.03 \pm 0.01 \text{ PgC yr}^{-1}$). This suggests that the mean CO_2 flux to the atmosphere may vary significantly from year to year (Figure 7).. In contrast, the atmospheric inversions (for the period 2001-2018) gave a much larger standard deviation than hindcast models suggesting that about 50% of the total Indian Ocean variability occurs in the NIO. The high variability in the atmospheric inversions may come from the period and region of atmospheric CO_2 data used in the models. The empirical models estimated lower IAV (0.03 to 0.12 PgC yr^{-1}) compared to hindcast and atmospheric inversion models.

To examine the IAV trends in the recent decades, the trends between 1985-2000 and 2001-2018 were compared. The IAV between 2001-2018 is lower ($-0.005 \pm 0.002 \text{ PgC yr}^{-1} \text{ decade}^{-1}$) than 1985-2000 ($-0.001 \pm 0.002 \text{ PgC yr}^{-1} \text{ decade}^{-1}$) by hindcast models suggesting that the source of the CO_2 to the atmosphere from the Arabian Sea is decreasing in the recent decades. This is possible that rapid warming of the western Arabian Sea was reported in recent decades (Roxy et al., 2015; Sridevi et al., 2023) resulting in weak vertical transport of CO_2 , and nutrients resulting in a decrease in primary

production (Dunstan et al., 2018; Roxy et al., 2016; Sridevi et al., 2023). A decline in Somali upwelling intensity and decreased evaporation due to the weakening of winds led to the warming of the Indian Ocean was reported in recent decades (D'Mello and Prasanna Kumar (2018). Sarma et al. (2000) estimated that vertical mixing is the major contributor to high pCO₂ levels and fluxes to the atmosphere in the Arabian Sea. The decrease in mixing may also weaken primary production resulting in an increase in CO₂ flux. Recently Sridevi et al. (2023) found that net primary production was decreasing only in the southern Arabian Sea (south of 12°N) whereas the decrease in nutrient inputs through mixing is compensated by increased atmospheric deposition of nutrients. Therefore, the weakening of upwelling intensity decreased the CO₂ source to the atmosphere in the past 4 decades in the Arabian Sea. The empirical models also simulated a decrease in the CO₂ fluxes from $-0.002 \pm 0.002 \text{ PgC yr}^{-1} \text{ decade}^{-1}$ in 1985-2000 to $-0.011 \pm 0.001 \text{ PgC yr}^{-1} \text{ decade}^{-1}$ in 2001-2018 and the magnitude of the decrease is higher than hindcast models. Nevertheless, this analysis suggests that the source of CO₂ to the atmosphere from the Arabian Sea is decreasing due to the warming of the basin leading to stratification and a decrease in upwelling intensity in the western basin.

3.3.3. Northeastern Indian Ocean (Bay of Bengal; BoB)

The IAV trends of pCO₂ simulated by hindcast and empirical models were close (1.54 ± 0.04 and $1.64 \pm 0.02 \text{ } \mu\text{atm yr}^{-1}$ respectively) between 1985 and 2018 in the BoB and these rates are almost close to that of in the Arabian Sea (Table 4). The pCO₂ growth rate increased between 1985 and 2000 (1.34 - $1.46 \text{ } \mu\text{atm yr}^{-1}$) to 2001-2018 (1.71 - $1.76 \text{ } \mu\text{atm yr}^{-1}$; Table 4) and it is consistent with the atmospheric growth rate (<https://gml.noaa.gov/ccgg/trends/>).

The IAV in the BoB simulated by the hindcast models is small (-0.02 to $+0.02 \text{ PgC yr}^{-1}$), and it is larger than the mean flux to the atmosphere from 1985 to 2018 ($0.00 \pm 0.02 \text{ PgC yr}^{-1}$). This suggests that the mean CO₂ flux to the atmosphere may vary from a net weak sink to a weak source to the atmosphere. The standard deviation is large suggesting that large IAV occurs in the BoB. In contrast, the atmospheric inversions showed a large standard deviation in comparison to hindcast models suggesting high IAV could occurs in the BoB (-0.03 to $+0.04 \text{ PgC yr}^{-1}$). On the opposite the empirical models showed low IAV in CO₂ fluxes (0.00 to 0.02 PgC yr^{-1}) and it is close to that of the annual mean flux to the atmosphere ($0.01 \pm 0.005 \text{ PgC yr}^{-1}$; Table 3). The empirical models estimated very low IAV compared to hindcast and atmospheric inversion models in the BoB (Figure 7).

The IAV in the CO₂ fluxes in the BoB from the hindcast models decreased from 1985-2000 ($-0.002 \pm 0.002 \text{ PgC yr}^{-1} \text{ decade}^{-1}$) to 2001-2018 ($-0.005 \pm 0.001 \text{ PgC yr}^{-1} \text{ decade}^{-1}$) but not statistically different. (Table 5). Similarly, empirical models simulated a decrease in the fluxes of CO₂ in the BoB

in recent decades (Table 5). The decrease of the CO₂ sink may be potentially caused by the deposition of atmospheric pollutants. Recently Sridevi and Sarma (2021) analyzed long-term trends (1998-2015) in pCO₂ levels in the BoB using an empirical model and noticed that pCO₂ decreased at the rate of -0.1 to -2.9 $\mu\text{atm yr}^{-1}$ in the central and eastern Bay associating with the decrease in salinity. The decrease in salinity is manifested by the melting of Himalayan glaciers due to climate change (Goes et al., 2020). In contrast, an increase in pCO₂ levels was noticed in the head bay and western BoB (0.1 to 2.4 $\mu\text{atm yr}^{-1}$) due to the deposition of atmospheric pollutants (Sarma et al., 2015; 2022). Therefore the decrease in the rate of CO₂ flux from the atmosphere in the recent decade may be caused by a decrease in salinity and deposition of atmospheric pollutants in the BoB.

3.3.4. Equatorial Indian Ocean (EIO)

The pCO₂ simulations displayed significant IAV by hindcast and empirical models in the equatorial Indian Ocean (1.65-1.72 $\mu\text{atm yr}^{-1}$) between 1985 and 2018. The enhanced pCO₂ growth rate was observed during the recent decade (2001-2018; 1.52-2.01 $\mu\text{atm yr}^{-1}$; Table 4) than between 1985 and 2000 (1.43-1.52 $\mu\text{atm yr}^{-1}$). The IAV in the CO₂ fluxes in the EIO simulated by the hindcast models is small (-0.11 to 0.06 PgC yr⁻¹), and it is larger than the mean flux to the atmosphere from 1985 to 2018 (-0.03±0.05 PgC yr⁻¹). The large standard deviation in the IAV by hindcast models suggested large variations in the CO₂ fluxes in the EIO and the mean CO₂ flux to the atmosphere may vary between weak sink to the source to the atmosphere. In contrast, both empirical and atmospheric inversion models displayed a decrease in the source for the past three decades. The hindcast models displayed a rate of decrease in CO₂ fluxes from the EIO between 1985-2000 (-0.004±0.005 PgC yr⁻¹ decade⁻¹) to 2001-2018 (-0.006±0.003 PgC yr⁻¹ decade⁻¹) whereas a decrease was also noticed by empirical models but the magnitude was higher (+0.01±0.003 and -0.018±0.002 PgC yr⁻¹ decade⁻¹ during 1985-2000 and 2001-2018 respectively). This analysis suggests that the CO₂ sink in the EIO is increasing in recent decades possibly due to the weakening of upwelling in the western basin due to rapid warming (D'Mello and Prasanna Kumar, 2018; Roxy et al., 2015) leading to less DIC import in surface.

3.3.5. The South Indian Ocean (SIO)

The IAV of pCO₂ simulated by hindcast and empirical models in the SIO were close (1.73±0.03 and 1.70±0.02 $\mu\text{atm yr}^{-1}$ respectively) between 1985 and 2018. The lower pCO₂ growth rate was observed between 1985 and 2000 (1.43-1.50 $\mu\text{atm yr}^{-1}$) while increased in the recent decades of 2001-2018 (1.91-1.98 $\mu\text{atm yr}^{-1}$ (Table 4). A slight increase in the surface ocean pCO₂ growth rate from north (Arabian Sea; 1.88±0.06 $\mu\text{atm yr}^{-1}$ between 2001-2018) to SIO (1.98±0.05 $\mu\text{atm yr}^{-1}$) was observed in

the hindcast models whereas such trends were not noticed in the empirical models (Table 4). In the period 1991–2007, Metzl (2009) calculated an oceanic pCO₂ growth rate of $2.11 \pm 0.11 \mu\text{atm yr}^{-1}$, which is $0.4 \mu\text{atm yr}^{-1}$ faster than in the atmosphere, suggesting that this region acts as a reducing sink of atmospheric CO₂. Recently Lo Monaco et al. (2021) reported increasing trends of pCO₂ in the southern Mozambique Channel ranging from $1.14 \mu\text{atm yr}^{-1}$ from 1963 to 1995, $1.70 \mu\text{atm yr}^{-1}$ from 1995 to 2004 and $2.41 \mu\text{atm yr}^{-1}$ from 2004 to 2019, and these rates are close to that of atmospheric CO₂ trend. The growth rate of pCO₂ estimated by both hindcast and empirical models appears close to that of measured values in the SIO (Metzl, 2009; Lo Monaco et al., 2021; Leseurre et al., 2022).

The IAV in the SIO by the hindcast models is small (-0.41 to $-0.03 \text{ PgC yr}^{-1}$), and it is larger than the mean flux to the atmosphere from 1985 to 2018 ($-0.03 \pm 0.05 \text{ PgC yr}^{-1}$). The large standard deviation in the IAV by hindcast models suggested large variations in the CO₂ fluxes in the SIO and the mean CO₂ flux to the atmosphere may vary between weak sink to the source to the atmosphere. In contrast, the empirical model did not show large variability but atmospheric inversion models displayed large standard deviations (Figure 7) with a higher increase in the sink from -0.4 to $-0.45 \text{ PgC yr}^{-1}$ between 2001 and 2018. The hindcast models displayed a decrease in CO₂ fluxes from the SIO between 1985–2000 ($-0.02 \pm 0.006 \text{ PgC yr}^{-1} \text{ decade}^{-1}$) to 2001–2018 ($-0.006 \pm 0.005 \text{ PgC yr}^{-1} \text{ decade}^{-1}$) whereas a decrease was also noticed by empirical models but the magnitude was higher (-0.003 ± 0.005 to $-0.012 \pm 0.004 \text{ PgC yr}^{-1} \text{ decade}^{-1}$ during 1985–2000 and 2001–2018 respectively).

3.4. Role of climate variability on CO₂ flux

The IAV in sea-air CO₂ fluxes in the Indian Ocean has been linked to the IOD and ENSO. Valsala and Maksyutov (2013) reported a strong correlation between the IODZM and sea-air CO₂ flux IAV in the Arabian Sea and that the roles of these two (ENSO and IODZM) modes are complementary in the period 1985–2018. The strong IOD event occurred in 1994, 1997 and 2006 within the period considered in this study with a Dipole Mode Index (DMI) value >0.6 . The simulated IAV by hindcast models shows an annual mean higher CO₂ flux during 1994, 1997 and 2006 by 9–14% in the Arabian Sea whereas a decrease by 5–30% was noticed in other regions (BoB; EIO and SIO) than in adjacent years. This is consistent with earlier observations (Sarma, 2006; Valsala and Maksyutov, 2013). Interestingly, empirical models displayed an increase in CO₂ fluxes by 8% in 1994 but a decrease in flux by 10% was noticed between 1997 and 2006 compared to the normal period in the Arabian Sea. In contrast, a significant increase in CO₂ fluxes in the EIO by 3 to 45% was simulated by empirical models whereas a decrease of 6–30% was simulated by hindcast models. Jabaud-Jan et al. (2004) noticed sea-to-air fluxes in the subtropical zone (20°S–37°S) associated with warming in January 1998, when strong IOD occurred, compared to sink observed in the same region during 2000 suggesting warming induced by

IOD enhanced CO₂ fluxes to the atmosphere. However, neither hindcast nor empirical models captured these features. The monthly mean CO₂ fluxes simulated by hindcast and empirical models in the Indian Ocean, including in the Arabian Sea, did not show significant relation with Dipole Mode Index (DMI) between 1985 and 2018 suggesting that weak IOD may not have a significant impact on CO₂ fluxes in the Indian Ocean.

The strong ENSO event (index value >1.0) occurred in 1987, 1992, 1997, 2010 and 2016 within the period considered in this study. During these events increase in annual mean CO₂ fluxes by 6-26% was observed in the Arabian Sea and BoB whereas a decrease in CO₂ fluxes was noticed in the EIO and SIO by hindcast models. In contrast, empirical models showed a decrease in CO₂ fluxes in the ENSO years in the Arabian Sea, BoB and SIO but an increase in the EIO. The monthly ENSO index displayed a significant linear correlation with CO₂ fluxes by hindcast models in the Arabian Sea and BoB ($p < 0.001$) but an insignificant relationship in the EIO and SIO ($p > 0.01$ and $p > 0.1$ respectively) whereas insignificant relation was observed with CO₂ fluxes by empirical models in all regions. Valsala and Maksyutov (2013) found a positive relationship between the ENSO index and CO₂ fluxes in the Arabian Sea and Southern Peninsular India. Nevertheless, this study suggests that empirical models did not capture either ENSO or IOD impacts on the CO₂ fluxes in the Indian Ocean.

Significant negative anomalies in the CO₂ fluxes were reported in the tropical Indian and Pacific Oceans and the absence of such anomaly was reported in the Southern Ocean (McKinley et al., 2020; Bennington et al., 2022). Bennington et al. (2022) reported an increase in >30% of the sink after the Pinatubo eruption. Interestingly significant decrease in CO₂ flux was observed between 1991 and the mean of 1992-93 in the Arabian Sea (0.038 and 0.032 PgC/y respectively), BoB (0.0033 and 0.002 PgC/y), EIO (-0.026 and -0.041) with decrease by 16 to 57% whereas it was smaller in the case of SIO (-0.18 and -0.19 PgC/y) associated with Pinatubo volcanic eruption (Fig. 7). These observations are consistent with the earlier studies (McKinley et al., 2020; Bennington et al., 2022). Recently Fay et al. (2023) reported high oxygen and carbon anomalies associated with Pinatubo volcanic eruptions for several years in the northern and tropical Pacific and tropical Indian Ocean but an insignificant impact is noticed in the Southern Ocean. The models used in this study also suggest an impact of the Pinatubo volcanic eruption on Indian Ocean CO₂ fluxes around 1991-1992 most pronounced in the EIO region (Fig. 7).

4. Conclusions

The Indian Ocean is severely under-sampled with reference to surface pCO₂ levels. In order to estimate the uptake of CO₂ by the Indian Ocean, CO₂ fluxes were simulated using several approaches, such as

a) hindcast, b) atmospheric inversions, and c) empirical models, were analyzed at different time scales and compared with spatially interpolated observations (called climatology). Our study suggests that the annual mean CO₂ uptake by the entire Indian Ocean (north of 37.5°S) for the period of 1985-2018 from all approaches varied between -0.27 and -0.13 PgC yr⁻¹ with a mean value of all models of -0.19±0.01 PgC yr⁻¹. The SIO (south of 18°S) region is a dominant annual sink for the atmospheric CO₂ with a mean of all models of -0.23±0.11 PgC yr⁻¹. In contrast, a mild source of CO₂ in the atmosphere was simulated by all models (0.02±0.05 PgC yr⁻¹) in the north of 18°S. The estimation of CO₂ uptake by the Indian Ocean was shown little variations among models.

All models simulated spatial variability in CO₂ fluxes in the Indian Ocean except for the underestimation of upwelling fluxes off Oman/Somalia coasts, and the EIO and overestimation of sink in the BoB due to poor monsoon mixing and freshwater discharge simulations in the hindcast models. The RHM have improved the simulation of CO₂ fluxes, compared to GHM, in these regions but has not reached close to the climatology. Variations in CO₂ fluxes by different models were also driven by variations in wind products, transfer velocity parameterization and atmospheric CO₂ data used in the flux estimations.

The atmospheric growth rate of pCO₂ was well simulated by all models and they captured the seasonal cycle in the sea-air CO₂ fluxes, however, the stronger amplitudes were simulated by all models than climatology. The empirical models simulated the seasonal cycle of sea-air CO₂ fluxes reasonably well with the observations. The difference between the hindcast and atmospheric inversion models and also in comparison with climatology may reflect errors in the model formulations and also poor observational data both in the atmosphere and ocean surface.

The inter-annual variability in CO₂ fluxes by the hindcast models is relatively weaker compared to the atmospheric inversions. The hindcast models suggest a slight weakening of the sink over the period of 1985-2018 in the SIO. In contrast, a decrease in the source of CO₂ in the atmosphere was simulated in the Arabian Sea, BoB and EIO by the hindcast and empirical models. It is difficult to conclude how models are performing about IAV due to the lack of time-series atmospheric and surface ocean pCO₂ observations. All models projected the influence of atmospheric extreme events, such as IODZM and ENSO on CO₂ fluxes in the Indian Ocean.

Unless the monsoon mixing is represented well in the models, it will remain difficult to confidently project the future changes in CO₂ fluxes in the Indian Ocean. The lack of seasonal data in most parts of the Indian Ocean is another serious problem to validate the models. Significant improvement in model performance was not noticed since the RECCAP1 comparison between models and

observations due to the lack of addition of new data in this region (Sarma et al., 2013). Therefore, intensive ocean observations of pCO₂ and atmospheric tower observations are required for further improvements of the models.

The Indian Ocean experiences extreme events such as eddies (Chen et al., 2012) and tropical cyclones and both cause enormous effluxes of CO₂ to the atmosphere that would influence local CO₂ fluxes (Byju and Prasanna Kumar, 2011; Ye et al., 2019). Swapna et al. (2022) projected an increase in cyclonic activity in the future in the Indian Ocean that may result in enhanced CO₂ fluxes at the air-sea interface. High resolution, with reference to space and time, is required to capture such features. The regional models are highly useful to capture such signatures than global models. It would be interesting to segregate the contribution of CO₂ fluxes due to an increase in cyclonic activity due to climate change.

Rapid warming of the Indian Ocean (Roxy et al., 2015) is experiencing and began to play an important role in global ocean heat uptake (Li et al, 2018). The decrease in the rate of warming due to aerosols was reported in the northern Indian Ocean (Sridevi et al., 2023). The decrease in the primary production in the western Indian Ocean (Roxy et al., 2016; Dalpadado et al., 2021; Sridevi et al., 2023), was reported due to the decline in wind speed and upwelling intensity. The lack of primary productivity trends due to an increase in the deposition of nutrients from the atmosphere was reported (Sarma et al., 2022; Sridevi et al., 2023). Rapid rate of ocean acidification was reported due to the atmospheric deposition of pollutants (Sarma et al., 2015; 2021; Kumar et al., 2022). Therefore the inclusion of atmospheric pollutants in the model improves the simulations of future changes in CO₂ fluxes significantly. Evaluating the changes in possible drivers due to climate change would be an interesting issue to look into in the future.

One serious drawback in the present study to use of observational climatology of CO₂ fluxes to compare with the model simulations. Due to a lack of observational data in the Indian Ocean, inter and extrapolations were done based on the advection-diffusion model (Takahashi et al., 2009). Recently Davis and Goyet (2021) suggested a new method to fill the gaps to balance the error in the undersampled regions. Utilizing such tools, as shown by Guglielmi et al. (2022 a, b), may further decrease errors associated with climatology and the evaluation of model simulations will be enhanced.

Acknowledgement: We would like to thank all the modellers who have supplied the model outcomes to perform this analysis. The RECCAP2 organizers are also thanked for organizing the meeting in Japan and also simulating discussions over the online platform to perform this exercise, especially Drs. Jens Daniel Mueller, Nicolas Gruber. NC is supported by the Arctic Challenge for Sustainability phase

II (ArCS-II; JPMXD1420318865) Projects of the Ministry of Education, Culture, Sports, Science and Technology (MEXT). PKP is partly supported by the Environment Research and Technology Development Fund (JPMEERF21S20800) of the Environmental Restoration and Conservation Agency of Japan. The INCOIS-BIO-ROMS regional Indian Ocean model has been configured as a part of the ‘Development of Climate Change Advisory Services’ project of the Indian National Centre for Ocean Information Services (INCOIS) under the ‘Deep Ocean Mission’ programme of the Ministry of Earth Sciences (MoES). This is INCOIS contribution number XXX. ZL is supported by Tamkeen through Research Institute grant CG009 to the NYUAD Arabian Center for Climate and Environmental Sciences (ACCESS). The Surface Ocean CO₂ Atlas (SOCAT, www.socat.info) used for empirical models is an international effort, endorsed by the International Ocean Carbon Coordination Project (IOCCP), the Surface Ocean Lower Atmosphere Study (SOLAS) and the Integrated Marine Biogeochemistry and Ecosystem Research program (IMBER), to deliver a uniformly quality-controlled surface ocean CO₂ database. We thank the two anonymous reviewers for making constructive suggestions, which resulted in improvements to this paper. This has NIO contribution number.....

Data availability statement

The data used in this study includes 14 hindcasts, 9 empirical and 2 atmospheric inversion model data submitted to Zenodo and freely available at doi.org/10.5281/zenodo.7787626 (Sarma et al., 2023).

References

- Al Azhar, M., Lachkar, Z., Lévy, M., & Smith, S. (2017). Oxygen minimum zone contrasts between the Arabian Sea and the Bay of Bengal implied by differences in remineralization depth. *Geophysical Research Letters*, 44(21), 11-106.
- Bakker, D. C., Pfeil, B., Landa, C. S., Metzl, N., O'brien, K. M., Olsen, A., et al. (2016). A multi-decade record of high-quality fCO₂ data in version 3 of the Surface Ocean CO₂ Atlas (SOCAT). *Earth System Science Data*, 8(2), 383-413.
- Bakker, D. C., Pfeil, B., Smith, K., Hankin, S., Olsen, A., Alin, S. R., et al. (2014). An update to the Surface Ocean CO₂ Atlas (SOCAT version 2). *Earth System Science Data*, 6(1), 69-90.
- Bakker, D. C. E., Alin, S. R., Bates, N., Becker, M., Castaño-Primo, R., Cosca, C. E., et al. (2020). Surface Ocean CO₂ Atlas Database Version 2020 (SOCATv2020)(NCEI accession 0210711). *NOAA National Centers for Environmental Information*. [Doi.org/10.25921/4xkx-ss49](https://doi.org/10.25921/4xkx-ss49). 2020.
- Bates, N. R., Pequignet, A. C., & Sabine, C. L. (2006). Ocean carbon cycling in the Indian Ocean: 1. Spatiotemporal variability of inorganic carbon and air-sea CO₂ gas exchange. *Global Biogeochemical Cycles*, 20(3).
- Behrenfeld, M. J., & Falkowski, P. G. (1997). Photosynthetic rates derived from satellite-based chlorophyll concentration. *Limnology and oceanography*, 42(1), 1-20.

- Bennington, V., Gloege, L., & McKinley, G. A. (2022). Variability in the global ocean carbon sink from 1959 to 2020 by correcting models with observations. *Geophysical Research Letters*, 49(14), e2022GL098632.
- Bettencourt, J. H., López, C., Hernández-García, E., Montes, I., Sudre, J., Dewitte, B., et al. (2015). Boundaries of the Peruvian oxygen minimum zone shaped by coherent mesoscale dynamics. *Nature Geoscience*, 8(12), 937-940.
- Bopp, L., Resplandy, L., Orr, J. C., Doney, S. C., Dunne, J. P., Gehlen, M., ... & Vichi, M. (2013). Multiple stressors of ocean ecosystems in the 21st century: projections with CMIP5 models. *Biogeosciences*, 10(10), 6225-6245.
- Brandt, P., Bange, H. W., Banyte, D., Dengler, M., Didwischus, S. H., Fischer, T., et al. (2015). On the role of circulation and mixing in the ventilation of oxygen minimum zones with a focus on the eastern tropical North Atlantic. *Biogeosciences*, 12(2), 489-512.
- Byju, P., & Kumar, S. P. (2011). Physical and biological response of the Arabian Sea to tropical cyclone Phyan and its implications. *Marine Environmental Research*, 71(5), 325-330.
- Canadell, J.G., P.M.S. Monteiro, et al. 2021. Global Carbon and other Biogeochemical Cycles and Feedbacks., in *Climate Change 2021: The Physical Science Basis. Contribution of Working Group I to the Sixth Assessment Report of the Intergovernmental Panel on Climate Change*, edited by L. G. Masson-Delmotte et al., Cambridge University Press.
- Chakraborty, K., Valsala, V., Bhattacharya, T., & Ghosh, J. (2021). Seasonal cycle of surface ocean pCO₂ and pH in the northern Indian Ocean and their controlling factors. *Progress in Oceanography*, 198, 102683.
- Chakraborty, K., Kumar, N., Girishkumar, M. S., Gupta, G. V. M., Ghosh, J., Udaya Bhaskar, T. V. S., & Thangaprakash, V. P. (2019). Assessment of the impact of spatial resolution on ROMS simulated upper-ocean biogeochemistry of the Arabian Sea from an operational perspective. *Journal of Operational Oceanography*, 12(2), 116-142.
- Chakraborty, K., Valsala, V., Gupta, G. V. M., & Sarma, V. V. S. S. (2018). Dominant biological control over upwelling on pCO₂ in sea east of Sri Lanka. *Journal of Geophysical Research: Biogeosciences*, 123(10), 3250-3261.
- Chandra, N., Patra, P. K., Niwa, Y., Ito, A., Iida, Y., Goto, D., et al. (2022). Estimated regional CO₂ flux and uncertainty based on an ensemble of atmospheric CO₂ inversions. *Atmospheric Chemistry and Physics*, 22(14), 9215-9243.
- Chau, T. T. T., Gehlen, M., & Chevallier, F. (2022). A seamless ensemble-based reconstruction of surface ocean pCO₂ and air-sea CO₂ fluxes over the global coastal and open oceans. *Biogeosciences*, 19(4), 1087-1109.
- Chen, G., Wang, D., & Hou, Y., (2012). The features and interannual variability mechanism of mesoscale eddies in the Bay of Bengal. *Continental Shelf Research*. 47, 178–185.
- Chevallier, F., Fisher, M., Peylin, P., Serrar, S., Bousquet, P., Bréon, F. M., et al. (2005). Inferring CO₂ sources and sinks from satellite observations: Method and application to TOVS data. *Journal of Geophysical Research: Atmospheres*, 110(D24).

- Cocco, V., Joos, F., Steinacher, M., Frölicher, T. L., Bopp, L., Dunne, J., et al. (2013). Oxygen and indicators of stress for marine life in multi-model global warming projections. *Biogeosciences*, 10(3), 1849-1868.
- Dalpadado, P., Arrigo, K. R., van Dijken, G. L., Gunasekara, S. S., Ostrowski, M., Bianchi, G., & Sperfeld, E. (2021). Warming of the Indian Ocean and its impact on temporal and spatial dynamics of primary production. *Progress in Oceanography*, 198, 102688.
- De Verneil, A., Lachkar, Z., Smith, S., & Lévy, M. (2022). Evaluating the Arabian Sea as a regional source of atmospheric CO₂: seasonal variability and drivers. *Biogeosciences*, 19(3), 907-929.
- D'Mello, J. R., & Prasanna Kumar, S. (2018). Processes controlling the accelerated warming of the Arabian Sea. *International Journal of Climatology*, 38(2), 1074-1086.
- Davis, D., and Goyet, C. 2021. Balanced error sampling with applications to ocean biogeochemical sampling, University of Perpignan, France, pp. 214.
- Dunstan, P. K., Foster, S. D., King, E., Risbey, J., O'Kane, T. J., Monselesan, D., et al. (2018). Global patterns of change and variation in sea surface temperature and chlorophyll a. *Scientific reports*, 8(1), 1-9.
- Fay, A. R., Gregor, L., Landschützer, P., McKinley, G. A., Gruber, N., Gehlen, M., et al. (2021). SeaFlux: harmonization of air–sea CO₂ fluxes from surface pCO₂ data products using a standardized approach. *Earth System Science Data*, 13(10), 4693-4710.
- Fay, A.R., McKinley, G.A., Lovenduski, N.S., Eddebbar, Y., Levy, M.N., Long, M.C., Olivarez, H.C., & Rustagi, R.R. (2023). Immediate and long-lasting impacts of the Mt. Pinatubo Eruption on Ocean oxygen and carbon inventories. *Global Biogeochemical Cycles*, 37, e2022GB007513.
- Friedlingstein, P., Jones, M. W., O'Sullivan, M., Andrew, R. M., Bakker, D. C., Hauck, J., et al. (2022). Global carbon budget 2021. *Earth System Science Data*, 14(4), 1917-2005.
- George, M. D., Kumar, M. D., Naqvi, S. W. A., Banerjee, S., Narvekar, P. V., De Sousa, S. N., et al. (1994). A study of the carbon dioxide system in the northern Indian Ocean during premonsoon. *Marine Chemistry*, 47(3-4), 243-254.
- Ghosh, S., Sinha, P., Bhatla, R., Mall, R. K., & Sarkar, A. (2022). Assessment of Lead-Lag and Spatial Changes in simulating different epochs of the Indian summer monsoon using RegCM4. *Atmospheric Research*, 265, 105892.
- Ghosh, J., Chakraborty, K., Bhattacharya, T., Valsala, V., & Baduru, B. (2022). Impact of coastal upwelling dynamics on the pCO₂ variability in the southeastern Arabian Sea. *Progress in Oceanography*, 203, 102785.
- Gloege, L., Yan, M., Zheng, T., & McKinley, G. A. (2022). Improved quantification of ocean carbon uptake by using machine learning to merge global models and pCO₂ data. *Journal of Advances in Modeling Earth Systems*, 14(2), e2021MS002620.
- Goes, J. I., Tian, H., Gomes, H. D. R., Anderson, O. R., Al-Hashmi, K., deRada, S., et al. (2020). Ecosystem state change in the Arabian Sea fuelled by the recent loss of snow over the Himalayan-Tibetan plateau region. *Scientific reports*, 10(1), 1-8.

- Goyet, C., Millero, F. J., O'Sullivan, D. W., Eiseheid, G., McCue, S. J., & Bellerby, R. G. J. (1998). Temporal variations of pCO₂ in surface seawater of the Arabian Sea in 1995. *Deep Sea Research Part I: Oceanographic Research Papers*, 45(4-5), 609-623.
- Gregor, L., Lebehot, A. D., Kok, S., & Scheel Monteiro, P. M. (2019). A comparative assessment of the uncertainties of global surface ocean CO₂ estimates using a machine-learning ensemble (CSIR-ML6 version 2019a)—have we hit the wall?. *Geoscientific Model Development*, 12(12), 5113-5136.
- Gregor, L., & Gruber, N. (2021). OceanSODA-ETHZ: a global gridded data set of the surface ocean carbonate system for seasonal to decadal studies of ocean acidification. *Earth System Science Data*, 13(2), 777-808.
- Gruber, N., Gloor, M., Mikaloff Fletcher, S. E., Doney, S. C., Dutkiewicz, S., Follows, M. J., et al. (2009). Oceanic sources, sinks, and transport of atmospheric CO₂. *Global biogeochemical cycles*, 23(1).
- Guglielmi V., F. Touratier, C. Goyet (2022a). Design of sampling strategy measurements of CO₂/carbonate properties. *Journal of Oceanography and Aquaculture*, 6(3): 000227. [doi:10.23880/ijoac-16000227](https://doi.org/10.23880/ijoac-16000227)
- Guglielmi V., F. Touratier, C. Goyet (2022b). Determination of discrete sampling locations minimizing both the number of samples and the maximum interpolation error: application to measurements of surface ocean properties. *Journal of Sea Research*, in revision
- Iida, Y., Takatani, Y., Kojima, A., & Ishii, M. (2021). Global trends of ocean CO₂ sink and ocean acidification: an observation-based reconstruction of surface ocean inorganic carbon variables. *Journal of Oceanography*, 77(2), 323-358.
- Jabaud-Jan, A., Metzl, N., Brunet, C., Poisson, A., & Schauer, B. (2004). Interannual variability of the carbon dioxide system in the southern Indian Ocean (20 S–60 S): The impact of a warm anomaly in austral summer 1998. *Global Biogeochemical Cycles*, 18(1).
- Körtzinger, A., Duinker, J. C., & Mintrop, L. (1997). Strong CO₂ emissions from the Arabian Sea during south-west monsoon. *Geophysical Research Letters*, 24(14), 1763-1766.
- Kumar, M. D., Naqvi, S. W. A., George, M. D., & Jayakumar, D. A. (1996). A sink for atmospheric carbon dioxide in the northeast Indian Ocean. *Journal of Geophysical Research: Oceans*, 101(C8), 18121-18125.
- Kumari, V. R., Sarma, V. V. S. S., Mahesh, G., & Sudheer, A. K. (2022). Temporal variations in the chemical composition of aerosols over the coastal Bay of Bengal. *Atmospheric Pollution Research*, 13(2), 101300.
- Kumari, V.R., Sarma, V.V.S.S. & Dileep Kumar, M. (2022). Spatial variability in aerosol composition and its seawater acidification potential in coastal waters of the western coastal Bay of Bengal. *Journal of Earth System Science*, doi.org/10.1007/s12040-022-01996-w.
- Kumari, V. R., Yadav, K., Sarma, V. V. S. S., & Dileep Kumar, M. (2021). Acidification of the coastal Bay of Bengal by aerosols deposition. *Journal of Earth System Science*, 130(4), 1-13.

- Kwiatkowski, L., Torres, O., Bopp, L., Aumont, O., Chamberlain, M., Christian, J. R., et al., (2020). Twenty-first century ocean warming, acidification, deoxygenation, and upper-ocean nutrient and primary production decline from CMIP6 model projections. *Biogeosciences*, 17(13), 3439-3470.
- Lachkar, Z., Lévy, M., & Smith, S. (2018). Intensification and deepening of the Arabian Sea oxygen minimum zone in response to increase in Indian monsoon wind intensity. *Biogeosciences*, 15(1), 159-186.
- Lachkar, Z., Mehari, M., Al Azhar, M., Lévy, M., & Smith, S. (2021). Fast local warming is the main driver of recent deoxygenation in the northern Arabian Sea. *Biogeosciences*, 18(20), 5831-5849.
- Lachkar, Z., Smith, S., Lévy, M., & Pauluis, O. (2016). Eddies reduce denitrification and compress habitats in the Arabian Sea. *Geophysical Research Letters*, 43(17), 9148-9156.
- Landschützer, P., Gruber, N., & Bakker, D. C. (2016). Decadal variations and trends of the global ocean carbon sink. *Global Biogeochemical Cycles*, 30(10), 1396-1417.
- Lauvset, S. K., Gruber, N., Landschützer, P., Olsen, A., & Tjiputra, J. (2015). Trends and drivers in global surface ocean pH over the past 3 decades. *Biogeosciences*, 12(5), 1285-1298.
- Leseurre, C., Lo Monaco, C., Reverdin, G., Metzl, N., Fin, J., Mignon, C., & Benito, L. (2022). Summer trends and drivers of sea surface fCO₂ and pH changes observed in the southern Indian Ocean over the last two decades (1998–2019). *Biogeosciences*, 19(10), 2599-2625.
- Li, Y., Han, W., Hu, A., Meehl, G. A., & Wang, F. (2018). Multidecadal changes of the upper Indian Ocean heat content during 1965–2016. *Journal of Climate*, 31(19), 7863-7884.
- Landschützer, P., Gruber, N., & Bakker, D. C. (2016). Decadal variations and trends of the global ocean carbon sink. *Global Biogeochemical Cycles*, 30(10), 1396-1417.
- Louanchi, F., Metzl, N., & Poisson, A. (1996). Modelling the monthly sea surface fCO₂ fields in the Indian Ocean. *Marine Chemistry*, 55(3-4), 265-279.
- Lo Monaco, C., Metzl, N., Fin, J., Mignon, C., Cuet, P., Douville, É., ... & Tribollet, A. (2021). Distribution and long-term change of the sea surface carbonate system in the Mozambique Channel (1963–2019). *Deep Sea Research Part II: Topical Studies in Oceanography*, 186, 104936.
- McKinley, G. A., Fay, A. R., Eddebbar, Y. A., Gloege, L., & Lovenduski, N. S. (2020). External forcing explains recent decadal variability of the ocean carbon sink. *AGU Advances*, 1(2), e2019AV000149.
- Metzl, N. (2009). Decadal increase of oceanic carbon dioxide in Southern Indian Ocean surface waters (1991–2007). *Deep Sea Research Part II: Topical Studies in Oceanography*, 56(8-10), 607-619.
- Metzl, N., Beauverger, C., Brunet, C., Goyet, C., & Poisson, A. (1991). Surface water carbon dioxide in the southwest Indian sector of the Southern Ocean: a highly variable CO₂ source/sink region in summer. *Marine Chemistry*, 35(1-4), 85-95.
- Metzl, N., Lo Monaco, C., Leseurre, C., Ridame, C., Fin, J., Mignon, C., et al. (2022). The impact of the South-East Madagascar Bloom on the oceanic CO₂ sink. *Biogeosciences*, 19(5), 1451-1468.

- Metzl, N., Louanchi, F., & Poisson, A. (1998). Seasonal and interannual variations of sea surface carbon dioxide in the subtropical Indian Ocean. *Marine Chemistry*, 60(1-2), 131-146.
- Metzl, N., Poisson, A., Louanchi, F., Brunet, C., Schauer, B., & Bres, B. (1995). Spatio-temporal distributions of air-sea fluxes of CO₂ in the Indian and Antarctic Oceans: A first step. *Tellus B*, 47(1-2), 56-69.
- Millero, F. J., Degler, E. A., O'Sullivan, D. W., Goyet, C., & Eiseid, G. (1998). The carbon dioxide system in the Arabian Sea. *Deep Sea Research Part II: Topical Studies in Oceanography*, 45(10-11), 2225-2252.
- Miyama, T., Kominami, Y., Tamai, K., Nobuhiro, T., & Goto, Y. (2003). Automated foliage chamber method for long-term measurement of CO₂ flux in the uppermost canopy. *Tellus B: Chemical and Physical Meteorology*, 55(2), 322-330.
- Mukhopadhyay, S. K., Biswas, H., De, T. K., Sen, S., & Jana, T. K. (2002). Seasonal effects on the air–water carbon dioxide exchange in the Hooghly estuary, NE coast of Bay of Bengal, India. *Journal of Environmental Monitoring*, 4(4), 549-552.
- Murtugudde, R., & Busalacchi, A. J. (1999). Interannual variability of the dynamics and thermodynamics of the tropical Indian Ocean. *Journal of Climate*, 12(8), 2300-2326.
- Murtugudde, R., McCreary Jr, J. P., & Busalacchi, A. J. (2000). Oceanic processes associated with anomalous events in the Indian Ocean with relevance to 1997–1998. *Journal of Geophysical Research: Oceans*, 105(C2), 3295-3306.
- Papa, F., Bala, S. K., Pandey, R. K., Durand, F., Gopalakrishna, V. V., Rahman, A., & Rossow, W. B. (2012). Ganga-Brahmaputra river discharge from Jason-2 radar altimetry: an update to the long-term satellite-derived estimates of continental freshwater forcing flux into the Bay of Bengal. *Journal of Geophysical Research: Oceans*, 117(C11).
- Pfeil, B., Olsen, A., Bakker, D. C., Hankin, S., Koyuk, H., Kozyr, A., et al. (2013). A uniform, quality controlled Surface Ocean CO₂ Atlas (SOCAT). *Earth System Science Data*, 5(1), 125-143.
- Poisson, A., Metzl, N., Brunet, C., Schauer, B., Bres, B., Ruiz-Pino, D., & Louanchi, F. (1993). Variability of sources and sinks of CO₂ in the Western Indian and Southern Oceans during the year 1991. *Journal of Geophysical Research: Oceans*, 98(C12), 22759-22778.
- Rödenbeck, C., Bakker, D. C., Gruber, N., Iida, Y., Jacobson, A. R., Jones, S., et al. (2015). Data-based estimates of the ocean carbon sink variability—first results of the Surface Ocean pCO₂ Mapping intercomparison (SOCOM). *Biogeosciences*, 12(23), 7251-7278.
- Rödenbeck, C., Keeling, R. F., Bakker, D. C., Metzl, N., Olsen, A., Sabine, C., & Heimann, M. (2013). Global surface-ocean pCO₂ and sea–air CO₂ flux variability from an observation-driven ocean mixed-layer scheme. *Ocean Science*, 9(2), 193-216.
- Roxy, M. K., Modi, A., Murtugudde, R., Valsala, V., Panickal, S., Prasanna Kumar, S., et al. (2016). A reduction in marine primary productivity driven by rapid warming over the tropical Indian Ocean. *Geophysical Research Letters*, 43(2), 826-833.

- Roxy, M. K., Ritika, K., Terray, P., Murtugudde, R., Ashok, K., & Goswami, B. N. (2015). Drying of Indian subcontinent by rapid Indian Ocean warming and a weakening land-sea thermal gradient. *Nature communications*, 6(1), 1-10.
- Sabine, C. L., Key, R. M., Johnson, K. M., Millero, F. J., Poisson, A., Sarmiento, J. L., et al. (1999). Anthropogenic CO₂ inventory of the Indian Ocean. *Global Biogeochemical Cycles*, 13(1), 179-198.
- Sabine, C. L., Wanninkhof, R., Key, R. M., Goyet, C., & Millero, F. J. (2000). Seasonal CO₂ fluxes in the tropical and subtropical Indian Ocean. *Marine Chemistry*, 72(1), 33-53.
- Saji, N. H., Goswami, B. N., Vinayachandran, P. N., & Yamagata, T. (1999). A dipole mode in the tropical Indian Ocean. *Nature*, 401(6751), 360-363.
- Sarma, V. V. S. S., Swathi, P. S., Kumar, M. D., Prasannakumar, S., Bhattathiri, P. M. A., Madhupratap, M., et al. (2003). Carbon budget in the eastern and central Arabian Sea: An Indian JGOFS synthesis. *Global Biogeochemical Cycles*, 17(4).
- Sarma, V. V. S. S. (2003). Monthly variability in surface pCO₂ and net air-sea CO₂ flux in the Arabian Sea. *Journal of Geophysical Research: Oceans*, 108(C8).
- Sarma, V. V. S. S. (2006). The influence of Indian Ocean Dipole (IOD) on biogeochemistry of carbon in the Arabian Sea during 1997–1998. *Journal of earth system science*, 115(4), 433-450.
- Sarma, V. V. S. S., Krishna, M. S., & Srinivas, T. N. R. (2020). Sources of organic matter and tracing of nutrient pollution in the coastal Bay of Bengal. *Marine Pollution Bulletin*, 159, 111477.
- Sarma, V. V. S. S., Krishna, M. S., Paul, Y. S., & Murty, V. S. N. (2015). Observed changes in ocean acidity and carbon dioxide exchange in the coastal Bay of Bengal—a link to air pollution. *Tellus B: Chemical and Physical Meteorology*, 67(1), 24638.
- Sarma, V. V. S. S., Krishna, M. S., Rao, V. D., Viswanadham, R., Kumar, N. A., Kumari, T. R., et al. (2012). Sources and sinks of CO₂ in the west coast of Bay of Bengal. *Tellus B: Chemical and Physical Meteorology*, 64(1), 10961.
- Sarma, V. V. S. S., Krishna, M. S., Srinivas, T. N. R., Kumari, V. R., Yadav, K., & Kumar, M. D. (2021). Elevated acidification rates due to deposition of atmospheric pollutants in the coastal Bay of Bengal. *Geophysical Research Letters*, 48(16), e2021GL095159.
- Sarma, V. V. S. S., Kumar, G. S., Yadav, K., Dalabehera, H. B., Rao, D. N., Behera, S., & Loganathan, J. (2019). Impact of eddies on dissolved inorganic carbon components in the Bay of Bengal. *Deep Sea Research Part I: Oceanographic Research Papers*, 147, 111-120.
- Sarma, V. V. S. S., Kumar, M. D., & George, M. D. (1998). The central and eastern Arabian Sea as a perennial source of atmospheric carbon dioxide. *Tellus B: Chemical and Physical Meteorology*, 50(2), 179-184.
- Sarma, V. V. S. S., Kumar, M. D., Gauns, M., & Madhupratap, M. (2000). Seasonal controls on surface pCO₂ in the central and eastern Arabian Sea. *Journal of Earth System Science*, 109(4), 471-479.
- Sarma, V. V. S. S., Kumar, M. D., George, M. D., & Rajendran, A. (1996). Seasonal variations in inorganic carbon components in the central and eastern Arabian Sea. *Current Science*, 852-856.

- Sarma, V. V. S. S., Kumari, V. R., Srinivas, T. N. R., Krishna, M. S., Ganapathi, P., & Murty, V. S. N. (2018). East India Coastal Current controls the dissolved inorganic carbon in the coastal Bay of Bengal. *Marine Chemistry*, 205, 37-47.
- Sarma, V. V. S. S., Lenton, A., Law, R. M., Metzl, N., Patra, P. K., Doney, S., et al. (2013). Sea–air CO₂ fluxes in the Indian Ocean between 1990 and 2009. *Biogeosciences*, 10(11), 7035-7052.
- Sarma, V. V. S. S., Prasad, M. H. K., & Dalabehera, H. B. (2021). Influence of phytoplankton pigment composition and primary production on pCO₂ levels in the Indian Ocean. *Journal of Earth System Science*, 130(2), 1-16.
- Sarma, V. V. S. S., Rao, G. D., Viswanadham, R., Sherin, C. K., Salisbury, J., Omand, M. M., et al. (2016). Effects of freshwater stratification on nutrients, dissolved oxygen, and phytoplankton in the Bay of Bengal. *Oceanography*, 29(2), 222-231.
- Sarma, V.V.S.S., Sridevi, B., Metzl, N., Patra, P.K., Lachkar, Z., Kunal Chakraborty, Goyet, C., Levy, M., Mehari, M., Chandra, N. (2023). Air-sea fluxes of CO₂ in the Indian Ocean between 1985 and 2018: A synthesis based on observation-based surface CO₂, hindcast and atmospheric inversion models (Version 1) [dataset], Zenodo, doi.org/10.5281/zenodo.778726.
- Schott, F. A., & McCreary Jr, J. P. (2001). The monsoon circulation of the Indian Ocean. *Progress in Oceanography*, 51(1), 1-123.
- Schott, F. A., Dengler, M., & Schoenefeldt, R. (2002). The shallow overturning circulation of the Indian Ocean. *Progress in oceanography*, 53(1), 57-103.
- Schott, F. A., Xie, S. P., & McCreary Jr, J. P. (2009). Indian Ocean circulation and climate variability. *Reviews of Geophysics*, 47(1).
- Sridevi, B., & Sarma, V. V. S. S. (2021). Role of river discharge and warming on ocean acidification and pCO₂ levels in the Bay of Bengal. *Tellus B: Chemical and Physical Meteorology*, 73(1), 1-20.
- Sridevi, B, Sabira, Sk., & Sarma, V.V.S.S. (2023). Impact of ocean warming on net primary production in the northern Indian Ocean: role of aerosols and freshening of surface ocean. *Environmental Science and Pollution Research*, doi: 10.1007/s11356-023-26001-9.
- Sutton, A. J., Feely, R. A., Maenner-Jones, S., Musielwicz, S., Osborne, J., Dietrich, C., Monacci, N., Cross, J., Bott, R., Kozyr, A., Andersson, A. J., Bates, N. R., Cai, W.-J., Cronin, M. F., De Carlo, E. H., Hales, B., Howden, S. D., Lee, C. M., Manzello, D. P., McPhaden, M. J., Meléndez, M., Mickett, J. B., Newton, J. A., Noakes, S. E., Noh, J. H., Olafsdottir, S. R., Salisbury, J. E., Send, U., Trull, T. W., Vandemark, D. C., and Weller, R. A. (2019) Autonomous seawater pCO₂ and pH time series from 40 surface buoys and the emergence of anthropogenic trends, *Earth Syst. Sci. Data*, 11, 421-439, <https://doi.org/10.5194/essd-11-421-2019>.
- Swapna, P., Sreeraj, P., Sandeep, N., Jyoti, J., Krishnan, R., Prajeesh, A. G., et al. (2022). Increasing frequency of extremely severe cyclonic storms in the north Indian Ocean by anthropogenic warming and southwest monsoon weakening. *Geophysical Research Letters*, 49(3), e2021GL094650.
- Takahashi, T., Sutherland, S. C., Wanninkhof, R., Sweeney, C., Feely, R. A., Chipman, D. W., et al. (2009). Climatological mean and decadal change in surface ocean pCO₂, and net sea–air CO₂ flux over the global oceans. *Deep Sea Research Part II: Topical Studies in Oceanography*, 56(8-10), 554-577.

- Thompson, D. W., & Solomon, S. (2002). Interpretation of recent Southern Hemisphere climate change. *Science*, 296(5569), 895-899.
- Valsala, V., & Maksyutov, S. (2013). Interannual variability of the air–sea CO₂ flux in the north Indian Ocean. *Ocean Dynamics*, 63(2), 165-178.
- Valsala, V., Sreeush, M. G., & Chakraborty, K. (2020). The IOD impacts on the Indian Ocean Carbon cycle. *Journal of Geophysical Research: Oceans*, 125(11), e2020JC016485.
- Valsala, V., Sreeush, M. G., Anju, M., Sreenivas, P., Tiwari, Y. K., Chakraborty, K., & Sijikumar, S. (2021). An observing system simulation experiment for Indian Ocean surface pCO₂ measurements. *Progress in Oceanography*, 194, 102570.
- Wanninkhof, R. (1992). Relationship between wind speed and gas exchange over the ocean. *Journal of Geophysical Research: Oceans*, 97(C5), 7373-7382.
- Wanninkhof, R. (2014). Relationship between wind speed and gas exchange over the ocean revisited. *Limnology and Oceanography: Methods*, 12(6), 351-362.
- Watson, A. J., Schuster, U., Shutler, J. D., Holding, T., Ashton, I. G., Landschützer, P., et al. (2020). Revised estimates of ocean-atmosphere CO₂ flux are consistent with ocean carbon inventory. *Nature communications*, 11(1), 1-6.
- Xie, S. P., Annamalai, H., Schott, F. A., & McCreary Jr, J. P. (2002). Structure and mechanisms of South Indian Ocean climate variability. *Journal of Climate*, 15(8), 864-878.
- Yadav, K., Rao, V. D., Sridevi, B., & Sarma, V. V. S. S. (2021). Decadal variations in natural and anthropogenic aerosol optical depth over the Bay of Bengal: the influence of pollutants from Indo-Gangetic Plain. *Environmental Science and Pollution Research*, 28(39), 55202-55219.
- Ye, H., Sheng, J., Tang, D., Morozov, E., Kalhor, M. A., Wang, S., & Xu, H. (2019). Examining the Impact of Tropical Cyclones on Air-Sea CO₂ Exchanges in the Bay of Bengal Based on Satellite Data and In Situ Observations. *Journal of Geophysical Research: Oceans*, 124(1), 555-576.
- Zhang, J., & Reid, J. S. (2010). A decadal regional and global trend analysis of the aerosol optical depth using a data-assimilation grade over-water MODIS and Level 2 MISR aerosol products. *Atmospheric Chemistry and Physics*, 10(22), 10949-10963.
- Zeng, J., Nojiri, Y., Landschützer, P., Telszewski, M., & Nakaoka, S. I. (2014). A global surface ocean CO₂ climatology based on a feed-forward neural network. *Journal of Atmospheric and Oceanic Technology*, 31(8), 1838-1849.

Table 1: Details of the hindcast models (including regional models) with reference to a period of the run, products used, parameterization of transfer velocity and resolution of the model.

Global hindcast model	Period for Analysis	Spun-up	Initial conditions/physical forcing	wind	Riverine input used	Transfer velocity	resolution
CCSM-WHOI	1958-2017						$1^0 \times 1^0$
CESM-ETHZ	1980-2018	Spun-up to preindustrial steady state with 287.4 ppm	POP2 model was initialized with Levitus data and state of rest Does not include the phosphoric and silicic acid systems	JRA	No	Wanninkhof 1992	$\sim 1^0 \times 1.125^0$
CNRM-ESM2-1	1980-2018	Preindustrial; 1850 global average CO2 set to 286.46 ppm	Physical: NCEP-2; air-sea flux data: CORE II; atm.CO2: GCP Global averaged annual CO2 Includes the phosphoric and silicic acid systems		Yes	Wanninkhof 2014	$1^0 \times 1^0$
EC-Earth3	1980-2018	Preindustrial steady state 284.32 ppm for 1850	O2, Nutrients: WOA13 DIC, Alkalinity: GLODAPv2; Freshwater input: OMIP2 from JRA1.4-55	JRA55	Yes	Wanninkhof 1992	1×1^0
FESOM_REcoM_LR (FESOM-1.4-REcoM2-LR)	1981-2019	Physical spun-up on HR mesh 1 with constant atm. CO2 BGC fields on LR mesh of 1980 year 278 ppm	atm.CO2: GCP Global averaged annual CO2 O2, Nutrients: WOA13 DIC, Alkalinity: GLODAPv2	JRA55	No	Wanninkhof 2014	$1^0 \times 1^0$
MOM6-Princeton	1980-2018	Atm. CO2 for preindustrial steady state: 278 ppm, Spun-up starting from 1959,	SST, SSS, nutrients: WOA13; DIC & Alkalinity: GLODAPv2; does not include Phosphoric and silicic acid systems. Alkalinity is influenced by inputs from river, calcium carbonate burial to the sediment and nitrogen redox change	JRA	Yes	Wanninkhof 1992	$0.5^0 \times 0.5^0$
MPIOM-HAMOCC	1980-2019	Preindustrial steady state 296.2 ppm atm.CO2	Atmospheric CO2 concentrations are according to the link provided in the RECCAP2 protocol Included phosphoric and silicic acid systems	NCEP	No	Wanninkhof 1992 & 2014	Bipolar grid with 1.5^0 near equator
MRI-ESM2-1	1980-2018	Preindustrial steady state 284.32 ppm	Initialized with those derived from GLODAPv2 and WOA13v2. SST, SSS, nutrients: WOA13v2	JRA 55	No	Wanninkhof 1992 & 2014	Nominally 100 km
NorESM-OC1.2	1980-2018	Preindustrial steady state	Nutrients: WOA13;		No	Wanninkhof 1992	Nominal 1^0

		for 1000 years CO2 set to 278 ppm	DIC and Alkalinity: GLODAPv2 Included phosphoric and silicic acid systems				
ORCA1_LIM3-PISCES (IPSL-NEMO-PISCES)	1980-2018	Initialized with observations in year 1836 and CO2 set to 286.46 ppm at 1870 level	DIC & Alkalinity GLODAPv2 Included phosphoric and silicic acid systems	JRA55	Yes	Wanninkhof 1992	1 ⁰ x 1 ⁰
ORCA025-GEOMAR	1980-2018	Preindustrial steady state for 137 years and CO2 set to 284.32 ppm	Levitus 1998; (SST & SSS) Nutrients: WOAv2 DIC & Alk: GLODAP Pre-spin-up for sea ice from different experiments	JRA55	No	Wanninkhof 1992	1/4 ⁰
Planktom12	1980-2018	Spun-up to 1750-1947 with looped 1990 NCEP forcing; Preindustrial steady state 278 ppm	NCEP forcing Sea-ice: NEMO-LIM2 model Included phosphoric and silicic acid systems			Wanninkhof 1992	1 ⁰ x 1 ⁰
Regional hindcast models							
INCOIS-BIO-ROMS	1980-2018	Initialized with observations for a particular year (1970) RECCAP2 Strategy 1	Atm.CO2: Keeling et.al., 1995 at monthly resolution. The physical state variables have been initialized using ECDA system simulated reanalysis data produced by GFDL. The biological state variables (NO3, Chlorophyll-a, O2, etc.) have been initialized using the climatological state of January generated from the climatological run of the model. The model state of the carbon state variables has been initialized using the Global Ocean Data Product (GLODAP; Key et al., 2004).	JRA55-do	Yes	Wanninkhof 2014	1/12 ⁰
ROMS-NYUAD	1980-2018	1950-1979 (repeated normal year for physical forcing, increasing pCO2 from Joos and Spahni (2008) and Keeling et al. (2005).	temp, salinity, u, v, SSH: ORAS5; O2 & nitrate: WOA18 Chl-a: CMEMS (SeaWiFS& MODIS) DIC & Alk, GLODAPv2	ERA-Interim	Yes	Wanninkhof 1992	0.1 x 0.1

Table 2: The methods used in the different observation-based surface CO₂ models used in this study.

Observation-based surface CO₂ models	Method	Reference
CMEMS-LSCE-FFNN	Feed Forward Neural Network (FFNN)	Chau et al., 2022
CSIRML6	Machine Learning/CSIR-ML6	Gregor et al., 2019
Jena-MLS (CarboScope)	/ocean mixed layer model	Rodenbeck et al., 2013
JMAMLR	Multiple Linear Regression model	Iida et al., 2021
SpcO2_LDEO HPD	Global Ocean Biogeochem Model/Extreme Gradient Boosting (XGB)	Gloege et al., 2022
SOMFNN	Neural Network	Landschutzer et al., 2016
NIES-MLR3	Feed Forward Neural Network (FFNN)	Zeng et al., 2014
OceanSODAETHZ	Geospatial Random Cluster Ensemble Regression (GRaCER)	Gregor and Gruber 2021
UOEX_WAT20	Multiple Linear Regression/ Feed Forward Neural Network (FFNN)	Watson et al., 2020

Table 3: The annual mean uptake (\pm standard deviation) of CO₂ from the climatology (Takahashi et al, 2009), hindcast, empirical and atmospheric inversion models. All units in PgC yr⁻¹. The negative values represent CO₂ flux into the ocean and the positive ones into the atmosphere.

Region	Climatology	Hindcast Models (Includes 2 Regional models) (n=14)	Observation- based models (n=9)	Atmospheric Inversion models (n=2)	All models (n=25)	Surface area (km ²)
Arabian Sea	0.08 \pm 0.06	0.03 \pm 0.01	0.08 \pm 0.01	0.16 \pm 0.12	0.06 \pm 0.05	0.70 x 10 ⁷
Bay of Bengal	0.01 \pm 0.01	-0.00 \pm 0.01	0.01 \pm 0.00	0.01 \pm 0.01	0.00 \pm 0.01	0.44 x 10 ⁷
Equatorial Indian Ocean	0.04 \pm 0.03	-0.05 \pm 0.04	0.02 \pm 0.02	0.02 \pm 0.03	-0.02 \pm 0.05	1.55 x 10 ⁷
South Indian Ocean	-0.20 \pm 0.16	-0.19 \pm 0.06	-0.23 \pm 0.02	-0.46 \pm 0.30	-0.23 \pm 0.11	1.24 x 10 ⁷
Indian Ocean	-0.07 \pm 0.14	-0.21 \pm 0.10	-0.13 \pm 0.04	-0.27 \pm 0.16	-0.19 \pm 0.10	3.92 x 10 ⁷

Table 4: The growth rate (\pm standard deviation) of pCO₂ ($\mu\text{atm yr}^{-1}$) in the different regions of the Indian Ocean and different periods. The p-value of the regression of time-series pCO₂ variability is given in bracket.

Period ($\mu\text{atm/yr}$)	Arabian Sea		Bay of Bengal		Equatorial Indian Ocean		South Indian Ocean		Indian Ocean	
	hindcast	Empirical	hindcast	Empirical	hindcast	Empirical	hindcast	Empirical	hindcast	Empirical
1985-2018	1.68 \pm 0.03 (7.7E-32)	1.64 \pm 0.02 (1.8E-39)	1.54 \pm 0.04 (5.4E-28)	1.64 \pm 0.02 (7.2E-38)	1.72 \pm 0.03 (1.1E-31)	1.65 \pm 0.02 (1.3E-38)	1.73 \pm 0.03 (1.8E-32)	1.70 \pm 0.02 (2.6E-37)	1.70 \pm 0.03 (4.6E-33)	1.67 \pm 0.02 (4.7E-39)
1985-2000	1.32 \pm 0.07 (3.7E-11)	1.41 \pm 0.04 (3.3E-15)	1.34 \pm 0.15 (5.2E-07)	1.46 \pm 0.05 (1.4E-13)	1.43 \pm 0.09 (1.6E-10)	1.52 \pm 0.04 (5.00E-15)	1.43 \pm 0.08 (6.9E-11)	1.50 \pm 0.05 (4.6E-14)	1.41 \pm 0.08 (2.9E-11)	1.49 \pm 0.04 (1.6E-15)
2001-2018	1.88 \pm 0.06 (2.1E-15)	1.76 \pm 0.03 (9.6E-21)	1.71 \pm 0.06 (1.6E-14)	1.76 \pm 0.05 (4.7E-17)	2.01 \pm 0.05 (5.2E-17)	1.82 \pm 0.04 (1.30E-17)	1.98 \pm 0.05 (9.4E-17)	1.91 \pm 0.03 (8.1E-21)	1.96 \pm 0.04 (3.9E-18)	1.84 \pm 0.03 (9.3E-20)

Table 5: Rate of changes in CO₂ fluxes (\pm standard deviation) (PgC yr⁻¹ decade⁻¹) in the Indian Ocean during different time periods. The p-value of the regression of time-series CO₂ variability is given in bracket. The negative values represent the decrease in source and vice versa for the positive.

Period	Arabian Sea		Bay of Bengal		Equatorial Indian Ocean		South Indian Ocean		Indian Ocean	
	hindcast	Empirical	hindcast	Empirical	hindcast	Empirical	hindcast	Empirical	hindcast	Empirical
1985-2018	-0.003 \pm 0.001 (3.5E-05)	-0.006 \pm 0.001 (2.7E-09)	-0.004 \pm 0.000 (2.4E-09)	-0.002 \pm 0.0001 (3.14E-05)	-0.007 \pm 0.001 (7.3E-06)	-0.006 \pm 0.002 (6.0E-04)	-0.010 \pm 0.002 (1.9E-05)	-0.008 \pm 0.002 (1.8E-05)	-0.023 \pm 0.003 (1.4E-08)	-0.021 \pm 0.003 (1.2E-07)
1985-2000	-0.001 \pm 0.002 (5.4E-01)	-0.002 \pm 0.002 (4.7E-01)	-0.002 \pm 0.002 (2.4E-01)	0.001 \pm 0.001 (2.3E-01)	-0.004 \pm 0.005 (3.7E-01)	0.010 \pm 0.003 (4.2E-03)	-0.020 \pm 0.006 (4.2E-03)	-0.003 \pm 0.005 (5.0E-01)	-0.028 \pm 0.012 (3.2E-02)	0.007 \pm 0.007 (3.7E-01)
2001-2018	-0.005 \pm 0.002 (7.8E-03)	-0.011 \pm 0.001 (1.8E-07)	-0.005 \pm 0.001 (3.0E-06)	-0.005 \pm 0.0001 (8.5E-09)	-0.006 \pm 0.003 (8.1E-02)	-0.018 \pm 0.002 (1.1E-07)	-0.006 \pm 0.005 (2.0E-01)	-0.012 \pm 0.004 (9.1E-03)	-0.023 \pm 0.007 (4.0E-03)	-0.046 \pm 0.005 (6.2E-08)

Figure 1: a) Figure showing the sub-regions of the Indian Ocean used in this study: South Indian Ocean (SIO; Brown), equatorial Indian Ocean (EIO; red), Arabian Sea (AS; Blue) and Bay of Bengal (BoB; green). b) shows the location of observations of oceanic pCO₂ collected since 1958 (Bakker et al., 2020), c) CO₂ flux climatology based on the observations and interpolated to a 4 x 5° grid (Takahashi et al., 2009) and d) Annual mean uptake from climatology, hindcast, empirical and atmospheric inversions models (PgC yr⁻¹) for the reference year of 2002. The error bars represent the standard deviation. The negative values represent fluxes into the ocean and positive to the atmosphere.

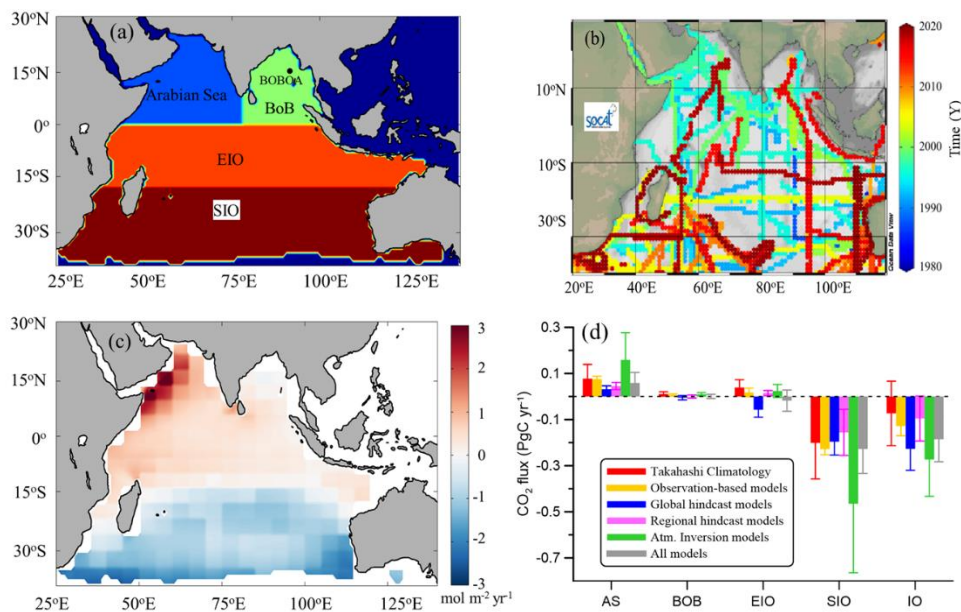


Figure 2: Annual mean uptake (in $\text{mol m}^{-2} \text{yr}^{-1}$) from the 14 hindcasts (2 regional) models for the reference year of 2002. The negative values reflect fluxes into the ocean and are positive for the atmosphere.

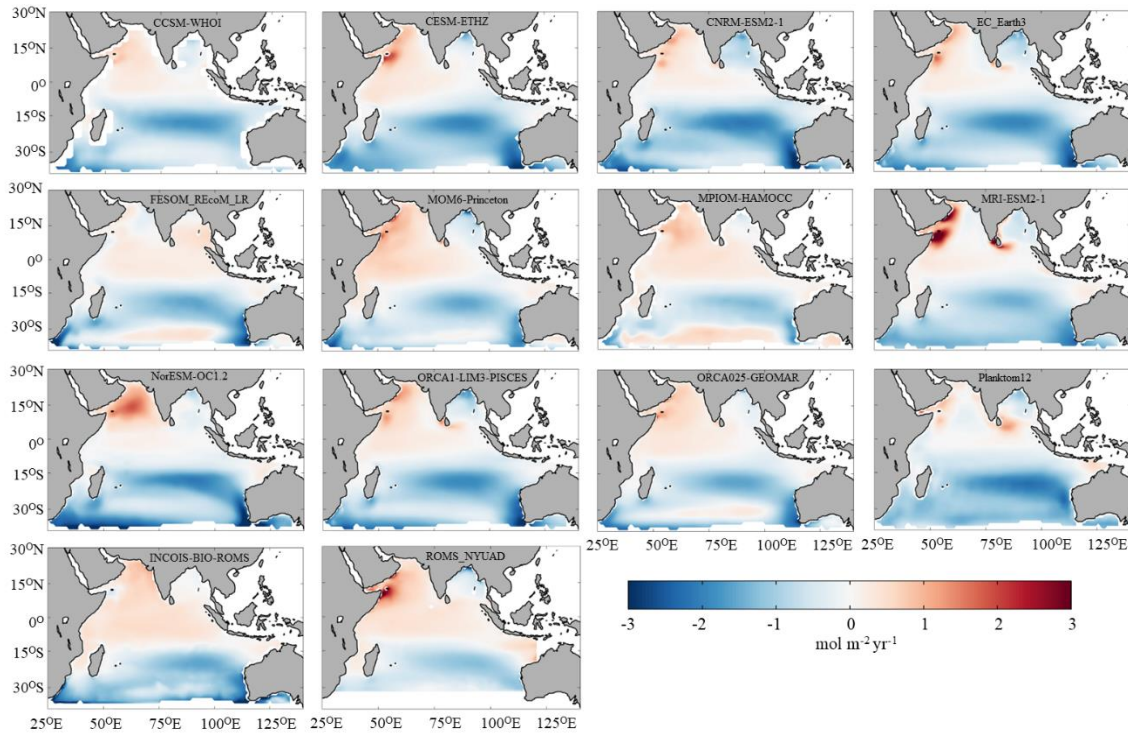


Figure 3: Annual mean uptake (in $\text{mol m}^{-2} \text{yr}^{-1}$) from the 9 observation-based models for the reference year of 2002. The negative values reflect fluxes into the ocean and are positive for the atmosphere.

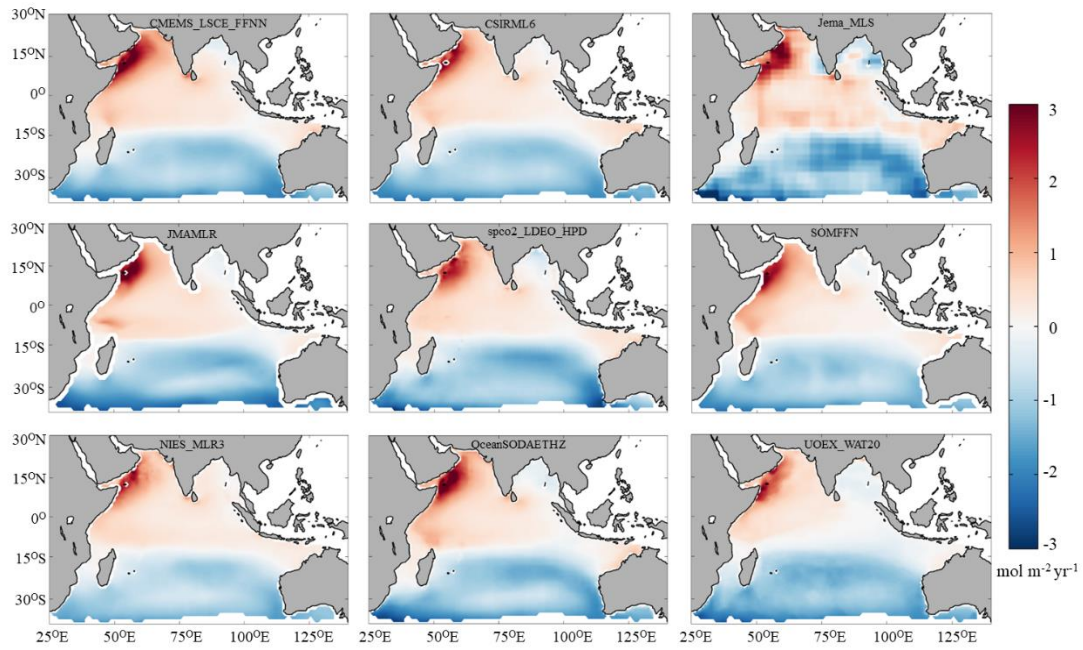


Figure 4: Annual mean uptake (in $\text{mol m}^{-2} \text{yr}^{-1}$) from the 2 atmospheric inversion models. The CAMSv20r1 used inter-annually varying prior fluxes from an empirical model CEMES, while MACTM used annually repeating prior flux seasonality from Takahashi et al. (2009). The negative values reflect fluxes into the ocean and are positive for the atmosphere.

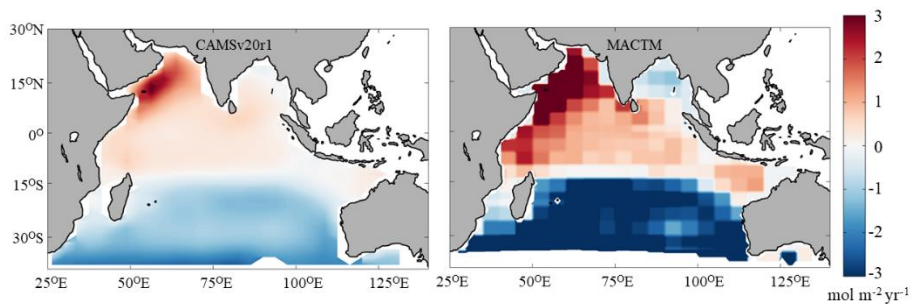


Figure 5: The zonally integrated, annual mean CO₂ uptake (30°N-37.5°S) from a) hindcast, b) empirical and c) atmospheric inversion models.

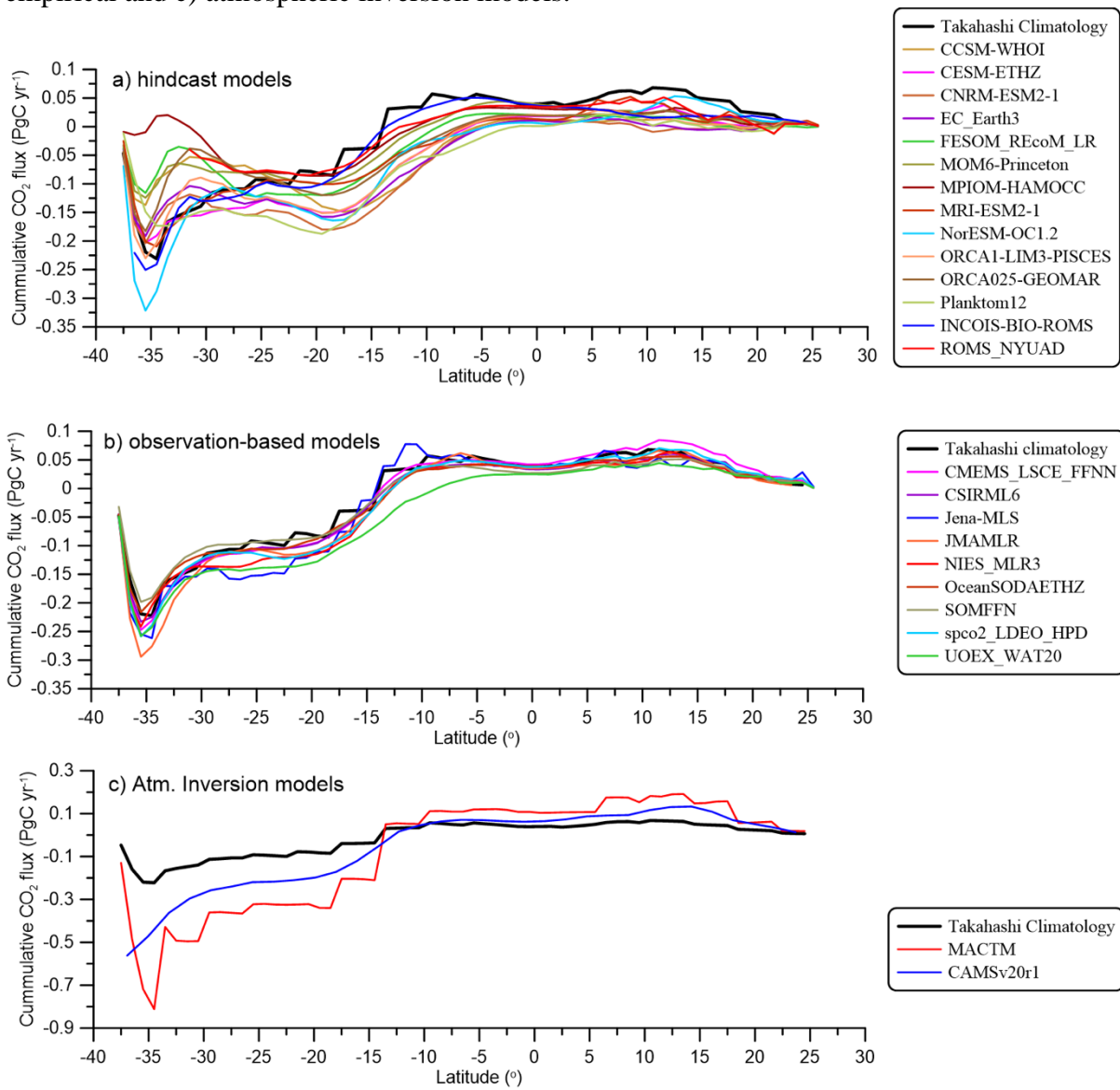


Figure 6: Seasonal cycle of the CO₂ fluxes (PgC yr⁻¹; left panel) and δpCO₂ (µatm; right panel) in the Indian Ocean from observations, mean hindcast, empirical and atmospheric inversion models in the Indian Ocean, Arabian Sea, BoB, EIO and SIO.

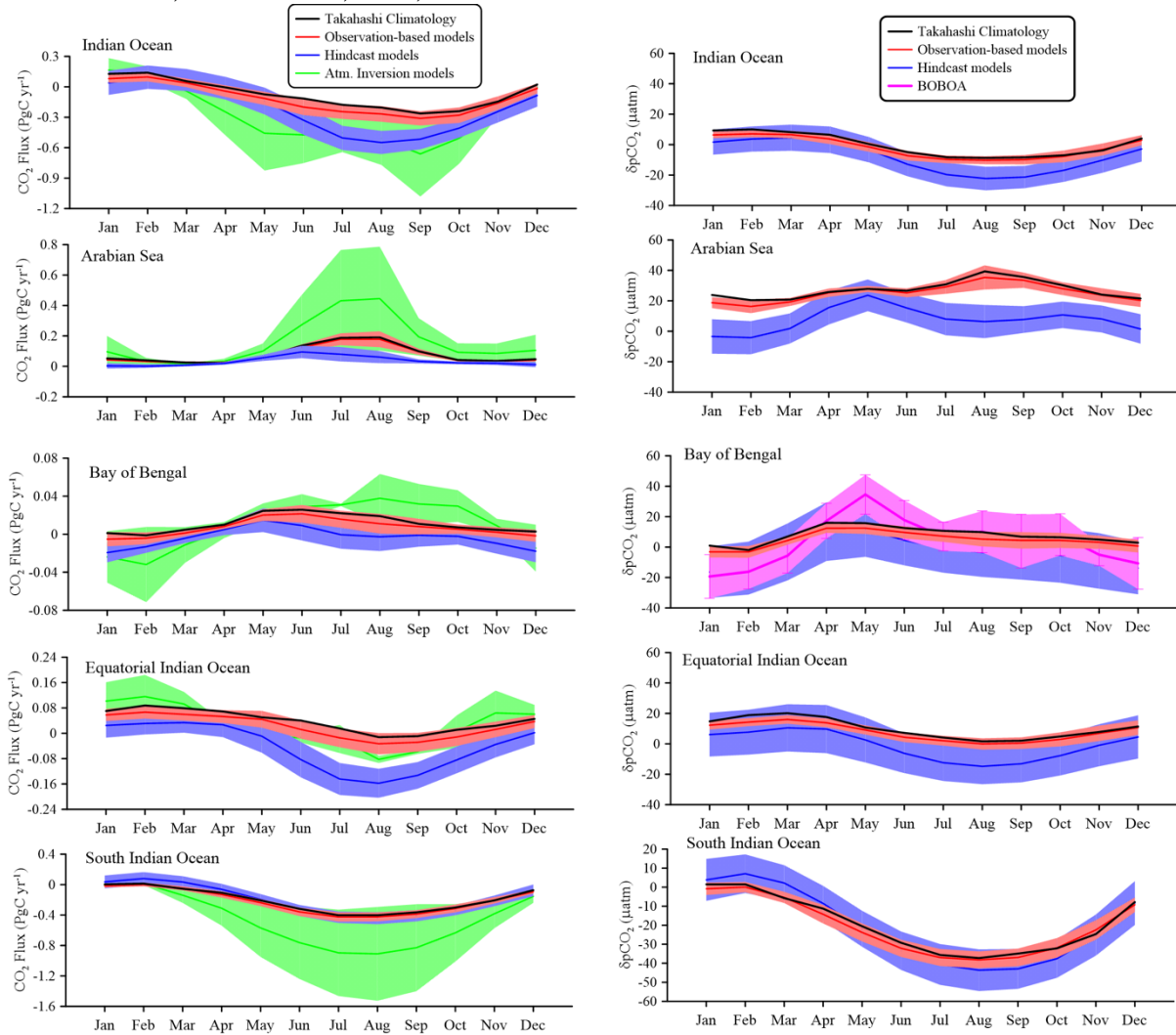
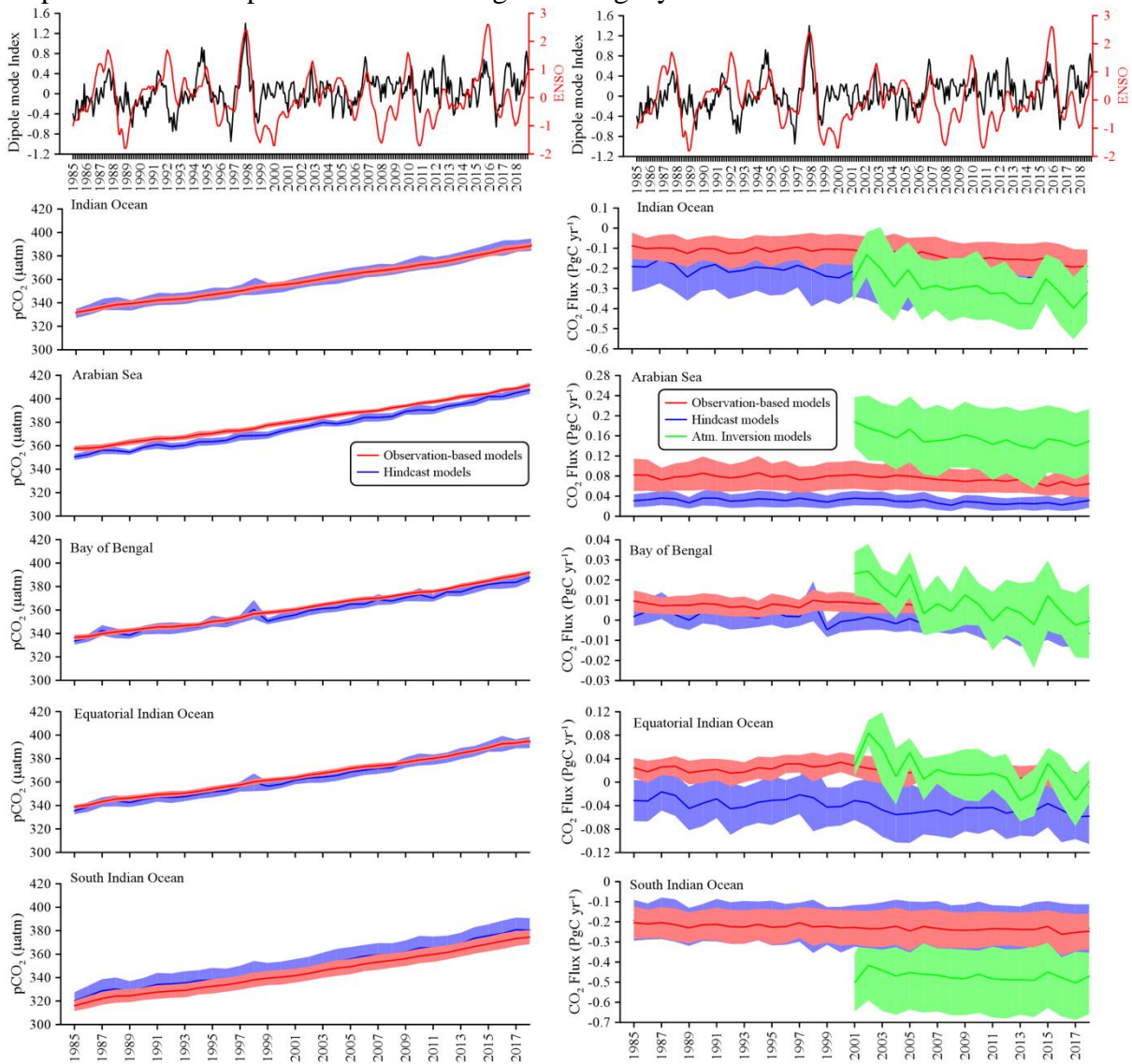
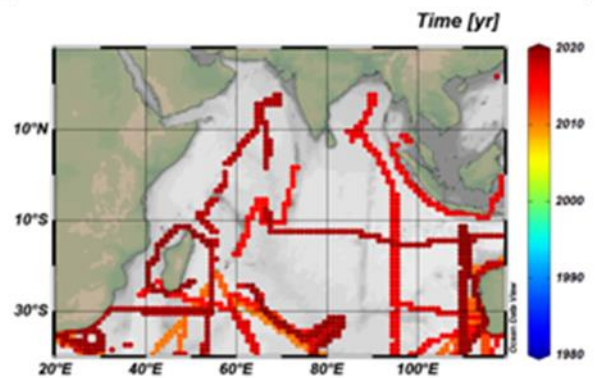
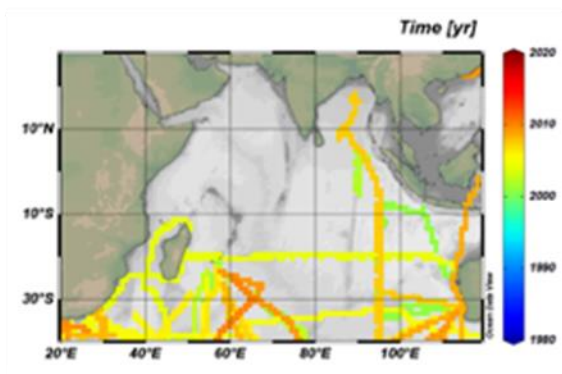
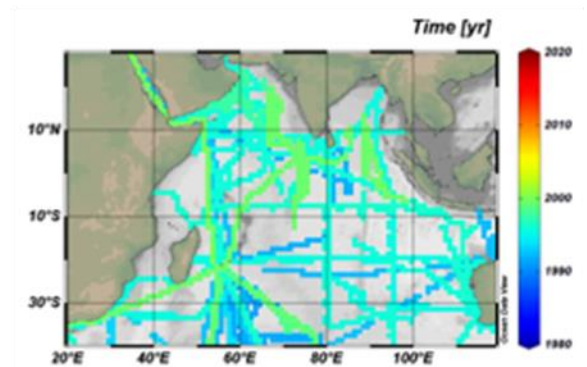
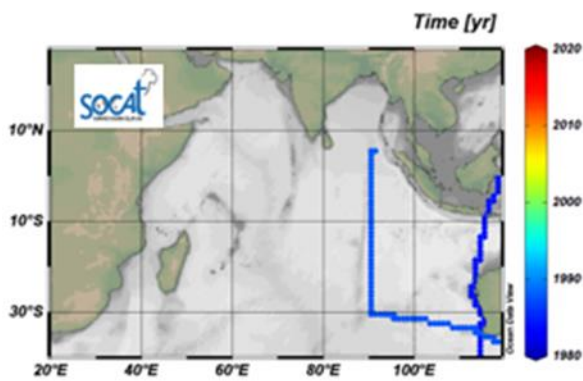


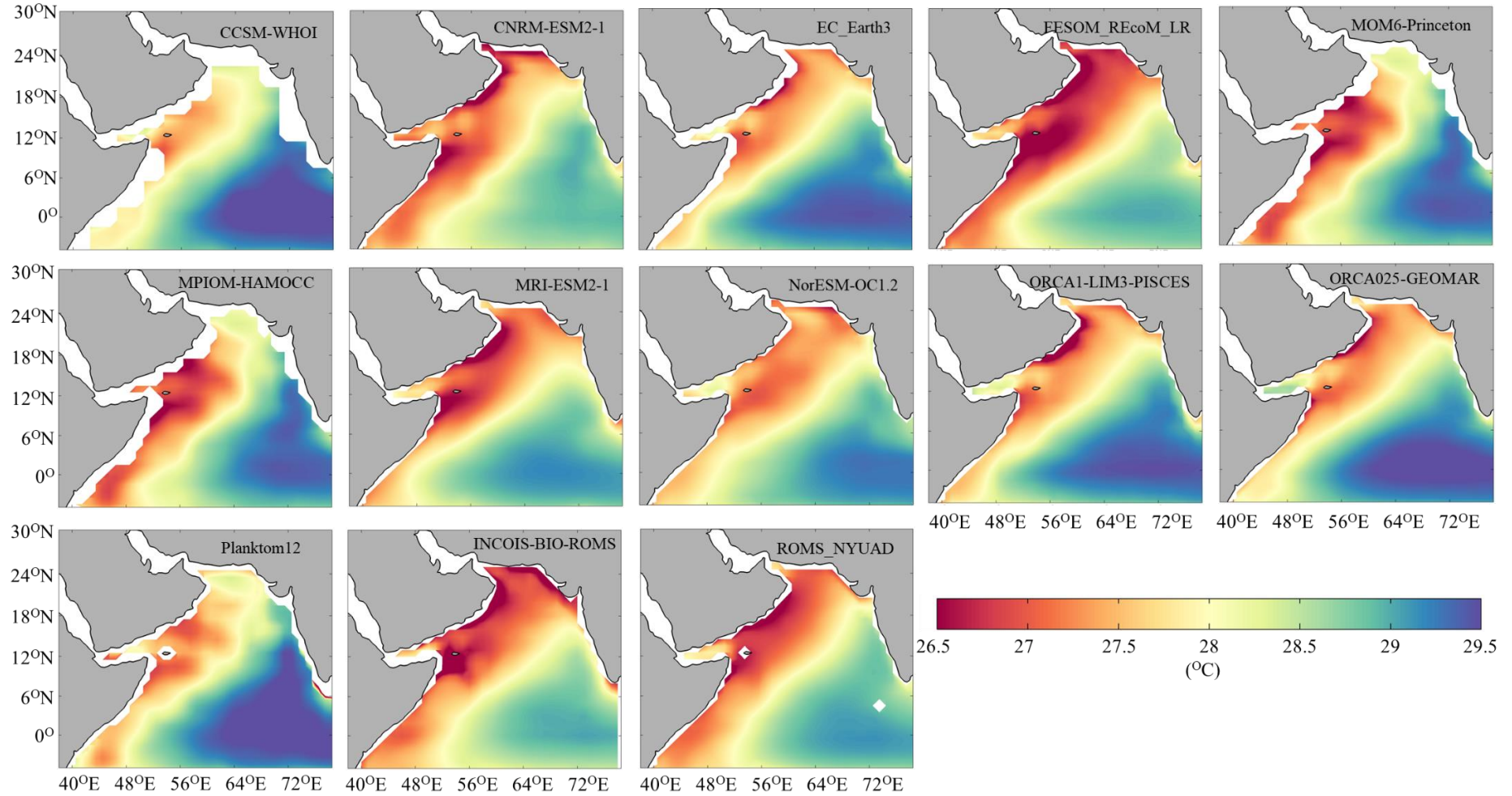
Figure 7: The inter-annual variability from hindcast, empirical and atmospheric inversion models. The upper panel shows the ENSO (<https://ggweather.com/enso/oni.htm>) and IOD index (<http://www.bom.gov.au/climate/iod/>) and the other panels for the entire Indian Ocean, Arabian Sea, Bay of Bengal, equatorial Indian Ocean, and South Indian Ocean. The trends of mean hindcast, empirical and atmospheric inversion are given in $\text{PgC yr}^{-1} \text{ decade}^{-1}$.



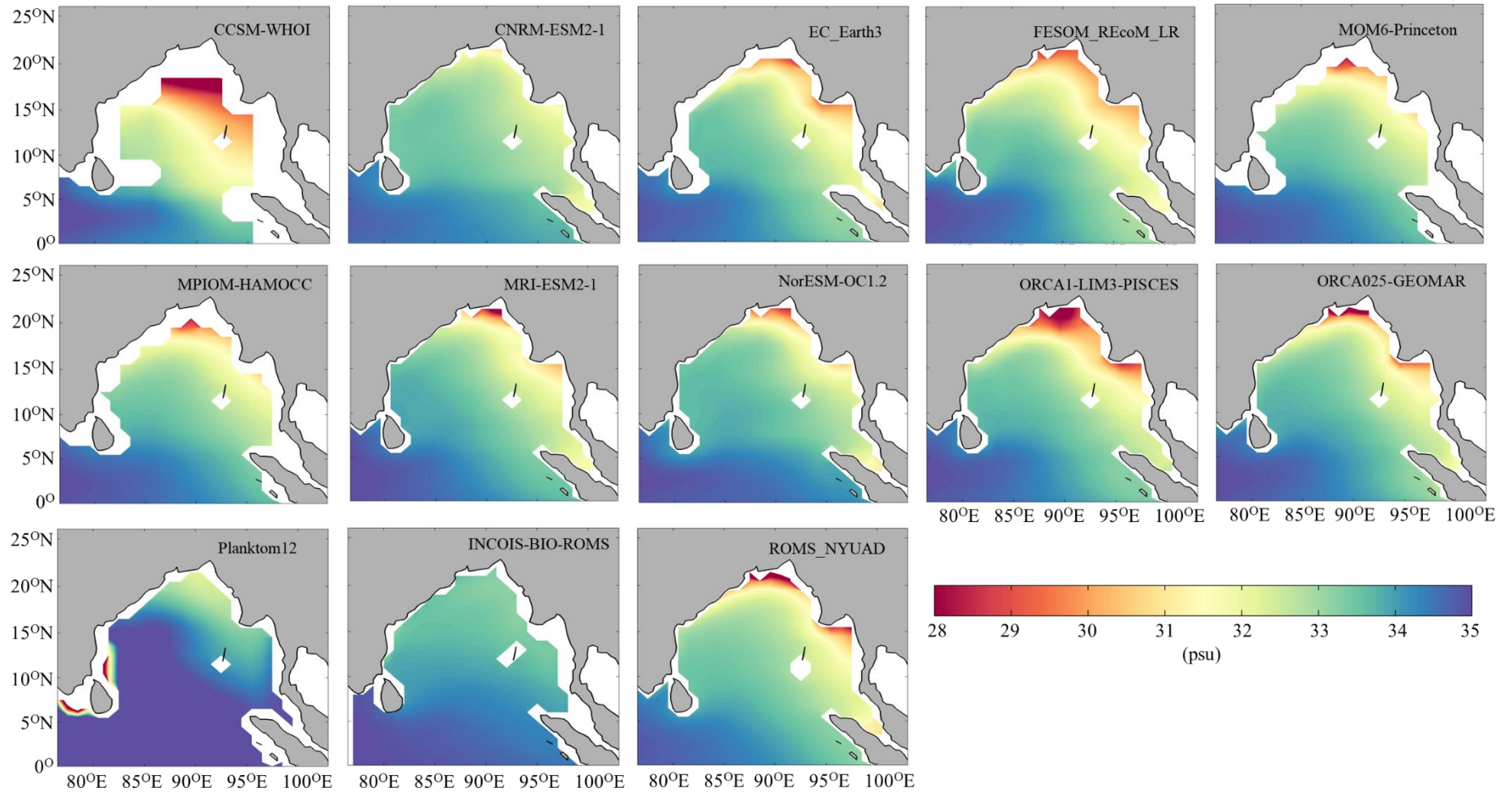
Supplementary Figure S1: Locations of pCO₂ data collected with reference to space and time are given in the Indian Ocean (Source: SOCAT, Bakker et al, 2020)



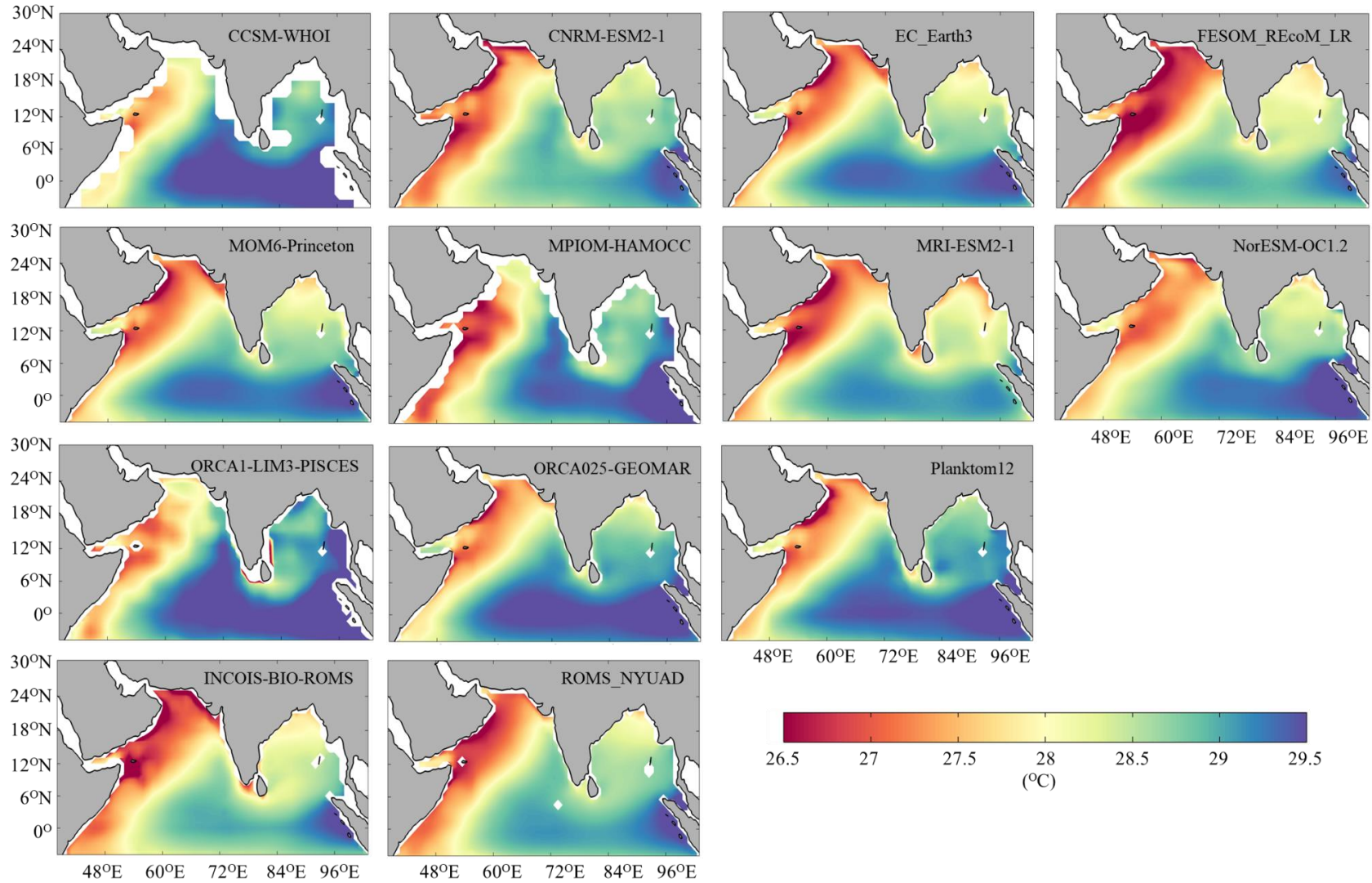
Supplementary Figure S2: The simulated mean sea surface temperature (1985-2018) by hindcast models in the Arabian Sea. Due to a lack of SST data from the CESM_ETHZ model, it was not included.



Supplementary Figure S3: The simulated mean sea surface salinity (1985-2018) by hindcast models in the Bay of Bengal. Due to a lack of SSS data from the CESM_ETHZ model, it was not included.



Supplementary Figure S4: The simulated mean sea surface temperature (1985-2018) by hindcast models in the Bay of Bengal. Due to a lack of SST data from the CESM_ETHZ model, it was not included.



Supplementary Figure S5: Seasonal cycle of the CO₂ flux (PgC yr⁻¹; left panel) and $\delta p\text{CO}_2$ (μatm ; right panel) from observations and hindcast models in the Indian Ocean, Arabian Sea, BoB, EIO and SIO.

